T.R.

GEBZE TECHNICAL UNIVERSITY

GRADUATE SCHOOL OF NATURAL AND APPLIED SCIENCES

FABRICATION OF ORGANIC/P-TYPE SEMICONDUCTING METAL OXIDE HYBRID STRUCTURES FOR GAS SENSING APPLICATIONS

ORHAN ŞİŞMAN

A THESIS SUBMITTED FOR MASTER OF SCIENCE

DEPARTMENT OF PHYSICS

GEBZE

2016

T.R.

GEBZE TECHNICAL UNIVERSITY

GRADUATE SCHOOL OF NATURAL AND APPLIED SCIENCES

FABRICATION OF ORGANIC/P-TYPE SEMICONDUCTING METAL OXIDE HYBRID STRUCTURES FOR GAS SENSING APPLICATIONS

ORHAN ŞİŞMAN

A THESIS SUBMITTED FOR THE DEGREE OF MASTER OF SCIENCE

DEPARTMENT OF PHYSICS

THESIS SUPERVISOR

PROF. DR. ZAFER ZİYA ÖZTÜRK

II. THESIS SUPERVISOR

ASSOC. PROF. DR. NECMETTİN KILINÇ

GEBZE

2016

T.C.
GEBZE TEKNİK ÜNİVERSİTESİ
FEN BİLİMLERİ ENSTİTÜSÜ

GAZ SENSÖR UYGULAMALARI İÇİN ORGANİK/P-TİPİ YARIİLETKEN METAL OKSİT HİBRİT YAPILARIN ÜRETİMİ

ORHAN ŞİŞMAN

YÜKSEK LİSANS TEZİ
FİZİK ANABİLİM DALI

DANIŞMANI
PROF. DR. ZAFER ZİYA ÖZTÜRK
II. DANIŞMANI
DOÇ. DR. NECMETTİN KILINÇ

GEBZE
2016

GEBZE TEKNİK ÜNİVERSİTESİ	**YÜKSEK LİSANS JÜRİ ONAY FORMU**

GTÜ Fen Bilimleri Enstitüsü Yönetim Kurulu'nun 27/06/2016 tarih ve 2016/43 sayılı kararıyla oluşturulan jüri tarafından 28/06/2016 tarihinde tez savunma sınavı yapılan Orhan Şişman'ın tez çalışması Fizik Anabilim Dalında YÜKSEK LİSANS tezi olarak kabul edilmiştir.

JÜRİ

ÜYE
(TEZ DANIŞMANI) : Prof. Dr. Zafer Ziya ÖZTÜRK

ÜYE : Prof. Dr. Savaş BERBER

ÜYE : Prof. Dr. Lütfi ARDA

ONAY

Gebze Teknik Üniversitesi Fen Bilimleri Enstitüsü Yönetim Kurulu'nun

...../...../..... tarih ve ...../..... sayılı kararı.

İMZA/MÜHÜR

SUMMARY

In this work, gas sensing properties of hybrid structures, composed of p-type semiconducting metal oxide nanowires and organic thin films, were investigated. Cu_2O and CuO nanowires were synthesized as p-type semiconducting metal oxide material. Cu_2O nanowires were fabricated with anodization in KOH+NH_4F aqeous solution and following thermal oxidation process. Their structural, optical, DC electrical characterizations were done and sensing properties against H_2 and NO_2 gas were investigated. CuO nanowires were fabricated with thermal oxidation on Si substrates. Sensor tests were performed against H_2 and ethanol gases after structural characterization of CuO nanowires. Zinc-pthlocyanine and fullerene functionalized poly(styrene-co-chloromethlystrene) (P(S-co-CMS-C_{60})) were used as organic materials. The hybrid heterostructures were synthesized with spin coating of dissolved organics in chloroform on Cu_2O and CuO nanowires. ZnPc@Cu_2O hybrid nanostructures showed better sensor response than Cu_2O nanowires against 0.5 ppm, 1 ppm, 2.5 ppm and 5 ppm NO_2 gas at 150 °C under dry air flow. While the sensor response of only ZnPc film decreased sharply against NO_2 gas at 150 °C under 38% relative humidity, the sensor response of ZnPc@Cu_2O hybrid structure increased. The sensor response of P(S-co-CMS-C_{60})@CuO hybrid structure and pure CuO nanowires were compared at 100 °C against 1000 ppm H_2 under dry air flow. It was observed that the hybrid structure increased the sensivity and sensor response.

Key Words: Metal Oxide, Organics Thin Films, Gas Sensors, Organic/Metal Oxide Hybrid Structures, Zinc-Phthalocyanine, Poly(styrene-co-chloromethlystrene).

ÖZET

Bu çalışmada p-tipi yarıiletken metal oksit nanotellerin organic ince filmler ile oluşturduğu hybrid yapıların gas algılama özellikleri incelenmiştir. P-tipi yarıiletken metal oksit malzeme olarak Cu_2O ve CuO nanoteller sentezlenmiştir. Cu_2O nanoteller, Cu filmin KOH + NH_4F sulu çözeltisi içerisinde anodizasyon ve sonrasında termal oksitleme işlemi ile oluşturulmuştur. Yapısal, optiksel, DC elektriksel karakterizasyonları yapılmış, H_2 ve NO_2 gazına karşı algılama özellikleri incelenmiştir. CuO nanoteller Si alttaş üzerine termal oksitleme yöntemiyle sentezlenmiştir. CuO nanotellerin yapısal karakterizasyonları yapılmış ve H_2, etanol gazına karşmı sensör testleri gerçekleştirilmiştir. Organic malzemeler olarak çinko fitalosiyanin (ZnPc) ve fulleren ile fonksiyanelleştirilmiş poly(styrene-co-chloromethlystrene) (P(S-co-CMS-C_{60})) kullanılmıştır. Kloroform ile çözülen organikler CuO ve Cu_2O nanoteller üzerine spin kaplama yöntemi ile kaplanarak hibrit heteroyapıları oluşturulmuştur. ZnPc@Cu_2O nanotel hibrit yapısının 150 °C'de 0.5 ppm, 1 ppm, 2.5 ppm ve 5ppm NO_2 gazına karşı kuru hava akışı altında Cu_2O nanotellerden daha iyi algılama gösterdiği gözlemlenlemiştir. Ayrıca 150 °C'de %38 bağıl nemin ZnPc filmin NO_2 gazına karşı algılamasını önemli miktarda düşürdüğü, ZnPc@Cu_2O hybrit yapısının algılamasını arttırdığı gözlemlenmiştir. P(S-co-CMS-C_{60})@CuO hybrit yapısının 100 °C'de 1000 ppm H_2 gazına karşı tepkisi sade CuO nanotellerin algılamasıyla karşılaştırılmıştır. Hybrit yapının algılamayı ve tepki hızını artırdığı gözlemlenmiştir.

Anahtar Kelimeler: Metal Oksit Malzemeler, Organik İnce Filmler, Gaz Sensörleri, Organik/Metal Oksit Hibrit Yapılar, Çinko-Fitalosiyanin, Poly(styrene-co-chloromethlystrene).

ACKNOWLEDGEMENT

I wish to express my profound gratitude and a sincere thanks to my research guides Prof. Zafer Ziya Öztürk and Assoc. Prof. Necmettin Kılınç, for valuable guidance and constant encouragement over the years. I would also thank to the Scientific Research Council of Turkey (TUBITAK) for providing financial support with the projects of "113F403" and "111M261".

I am grateful to Prof. Vefa Ahsen, Prof. Ayşe Gül Gürek, Prof. Faruk Yılmaz, Assoc. Prof. Devrim Atilla and Büşra Şennik, members of Gebze Technical University Chemistry Department, for their support with synthesizing organics.

I would like to thank Prof. Alberto Romano-Rodriguez and Jordi Sama, members of Barcelona University Electronics Department, for accepting me as visitor scientist in their laboratory with Short Term Scientific Mission (STSM) Program.

I express my indebtedness to Erdem Şennik and Onur Alev for sharing their ideas and experiences with me. They cheerfully answered all my questions on laboratory works, which was a great help throughout the study period.

It gives me pleasure to record my thanks to my family and my friend, Yasemin for their love, prayers, and moral supports. Their existence gives always me power to motivate my studies.

TABLE OF CONTENTS

LIST OF ABBREVIATIONS AND ACRONYMS

Abbreviations and Acronyms		**Explanations**
e^-	:	Electron
E_a	:	Activation energy
h	:	Planck constant
k_B	:	Boltzmann constant
k	:	Reaction rate constant
L_d	:	Debye length
n	:	Electrical charge concentration
O^-	:	Ionized Oxygen atom
O_2	:	Oxygen molecule
O_2^-	:	Ionized Oxygen molecule
O^{2-}	:	Double ionized Oxygen atom
$\frac{1}{2}O_2$	:	Oxygen atom
q	:	Electrical charge
R_a	:	Resistance in air
R_g	:	Resistance in active gas
R_{sensor}	:	Response of gas sensor
S_g	:	Sensitivity
t	:	Time
T	:	Temperature
V	:	Volt
V_m	:	Volume of material
V_s	:	Volume of system
W	:	Watt
α	:	Absorption coefficient
ε	:	Static dielectric constant
μ	:	Mikron
σ	:	Conductance

Γ	:	Time constant
Φ	:	Surface to volume ratio
ν	:	Frequency
CP	:	Conductive Polymer
CuPc	:	Cupper Phthalocyanine
CVD	:	Chemical Vapor Deposition
DC	:	Direct Current
GTU	:	Gebze Technical University
IDT	:	Interdigidated transducer
MOX	:	Metal Oxide
PAN	:	Polyacrylaonitrile
P(S-*co*-CMS-C_{60})	:	Fullerene functionalized poly(styrene-co-chloromethlystrene)
RF	:	Radio Frequency
RH	:	Relative Humidity
rpm	:	Rotates per minutes
sccm	:	Standart Cubic Centimeter per Unit
SEM	:	Scanning Electron Microscope
UV	:	Ultra Violet
VOCs	:	Volatile Organic Compounds
XPS	:	X-Ray Photoelectron Spectroscopy
XRD	:	X-Ray Diffraction
ZnPc	:	Zinc Phthalocyanine

LIST OF FIGURES

LIST OF TABLES

1. INTRODUCTION

Sensor is a device that can convert the physical or chemical changes in its environment to electrical signals. Sensor technology has a long history with the needs of industry to record physical parameters. In the beginning of 20th century, the emerging issues in test and measurement technology accelerated the research in semiconductor technology [1]. A gas sensor is a device in which one or more of its physical properties (e.g., mass, electrical conductivity, or capacitance) changes upon the exposure towards a gas species [1,2]. A slight change in these properties can be quantified and measured directly or indirectly. A typical gas sensor has two basic components, a sensing layer and a transducing platform. Gas molecules interact chemically with the sensing layer, which results in a change of the sensor's physical/chemical properties. The transducer then measures these changes and produces an electrical output signal [2]. A general view of gas sensor components is given below at table 1 includes types of sensing materials, types of transducers.

Table 1.1: General view of gas sensor components.

Sensing Layer Materials	**Transducer Types**
Metals	Optical
Semiconductors	Mass Sensitive
Organics	Electrochemical
Inorganic/organic hybrid structures	Conductometric

After the first discoveries of Heiland [3], Bielanski et al. [4] and Seiyama et al. [5] about metal oxide-gas reactions during 1950s, Taguchi brought MOX gas sensor as an industrial product (Taguchi type sensors) based on thick films of SnO_2 since 1960s [6,7]. The advantages of the MOX gas sensors such as reducible size, low-power-consumption, easy synthesis methods, good sensing properties and high compatibility with microelectronic processing have dominated the researches on this field [7-9].

1.1. Motivation

In last a few years, some studies showed that the some organic/inorganic hybrid structures can enhance the sensivity, selectivity and reduce working temperature of gas sensors [10-12]. The promising sensor results of hybrid structures have emerged the necessity of understanding the organic/metal oxides interface properties to more effective gas sensors. The idea of bringing together these metal oxides and organics opens new questions how change their conduction and sensing mechanism, what are the effecting factors on gas sensing. This study focused on the gas sensing properties of hybrid structures combination of organics@Cu_2O and organics@CuO.

1.2. Objectives

The aim of this work is to develop organics/p-type semiconducting CuO and Cu_2O hybrid structures for usage in gas sensor applications. This includes;

- Investigation of synthesis methods CuO and Cu_2O nanowires.
- Synthesis of organics/1D nanostructures of cuprous oxides (Cu_2O) and copper oxides (CuO) hybrid structures.
- Understanding the sensing mechanism behind the interaction of gas species with organic/p-type metal oxide hybrid surfaces.

2. GENERAL INFORMATION

2.1. Metal Oxide Nanowires Based Gas Sensors

2.1.1. Metal Oxides Nanowires

Semiconductor metal oxides offer a stable, selective and sensitive layer. In 1991, Yamazoe showed that reduction of crystallite size went along with a significant increase in sensor performance [13]. Nanostructures increase efficiency the surface area with their high aspect ratio, low limit of detection and low response time for metal oxide based gas sensors [6,7,14-16]. Thus, the technological challenge has moved to the fabrication of materials with small crystallizes size which maintained their stability over long-term operation at high temperature. Nanotechnology has supported the gas sensor technology by reducing size, power consumption, and increasing sensors' performance for a wide range of applications [17-19].

Metal oxides are ceramic materials which their starting materials are abundant and cheap. The one of the most important reason of extensive usage of MOXs in many fields is their stability in many media. Moreover, they have many easy and low cost synthesis methods such as thermal oxidation, electrochemical, hydrothermal, chemical vapor deposition (CVD) etc. for desired nano and micro structures. This variety of synthesis methods has dominated the researches on MOX nanowires based gas sensors.

The semiconducting behavior of MOXs arises from deviation of stoichiometry. Doping aliovalent cations or oxygen-nonstoichiometry determine the majority of charge carriers in wide-bandgap oxide semiconductors and also the type of semiconductor [20]. While the deficiency of metal ions in the undoped NiO cause to p-type semiconductivity, the formation of oxygen vacancies in undoped SnO_2 cause to n-type semiconductivity.

Most of the MOX based gas sensor studies were dedicated to n-type semiconductor metal oxides because of their superior surface properties. The figure 2.1. shows the pie chart of studies based on MOXs to give an idea of the usage on gas sensors.

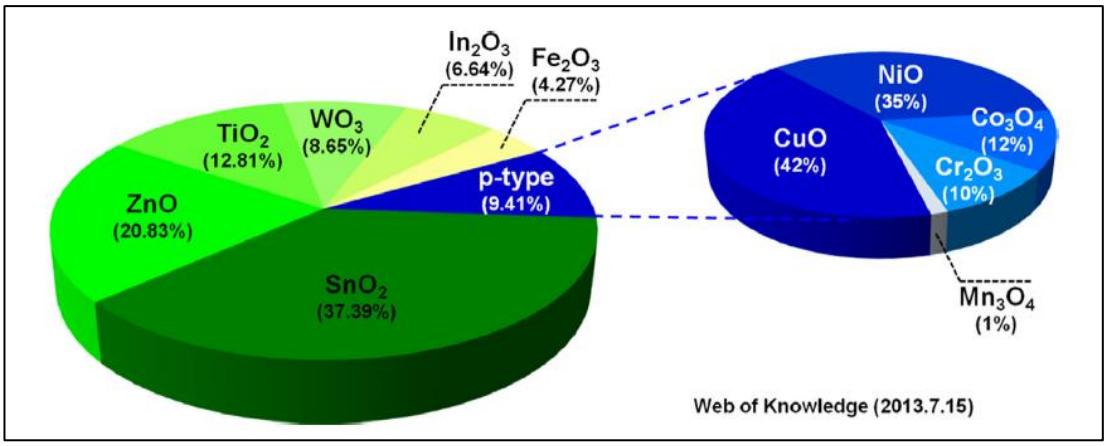

Figure 2.1: Studies on metal oxide semiconductor gas sensors.

While n-type semiconductor MOXs like SnO_2, TiO_2, ZnO etc. offer higher sensivity to some gases, they need higher working temperature and have less selectivity values than p-types. On the other hand, p-type MOXs have taken attention with their low working temperature and higher selectivity values.

2.1.2. Sensing Mechanism of MOX Nanowires

The working temperatures of MOX gas sensors are in the temperature range 100-500 °C. The oxygen molecules are adsorbed on MOX surface and form oxygen ion molecules by attracting an electron from the conduction band of MOX as shown in the equation (2.1) when the MOX is heated at temperature range 100-200 °C. Above this temperature range, the oxygen molecules are dissociated into oxygen ion atoms with singly or doubly negative electric charges by attracting an electron again from the conduction band as shown in the equation (2.2) and (2.3).

$$O_{2(gas)} + e^- \leftrightarrow O^-_{2(adsorbed)} \tag{2.1}$$

$$\frac{1}{2}O_2 + e^- \overset{k_{Oxy}}{\Longleftrightarrow} O^-_{ads} \tag{2.2}$$

$$\frac{1}{2}O_2 + 2e^- \overset{k_{Oxy}}{\Longleftrightarrow} O^{2-}_{ads} \tag{2.3}$$

where the k_{gas} is the reaction rate constant [21]. The effect of oxygen ionosorption causes the electron depletion region for n-type MOX and hole accumulation region for p-type gas sensors. Oxygen ions give up the electrons from the surface back to the conduction band of MOX when the active oxygen ions on the surface meet the target gas molecule. A schematic representation of the conduction mechanism for n-type and p-type MOX is given at figure 2.2.

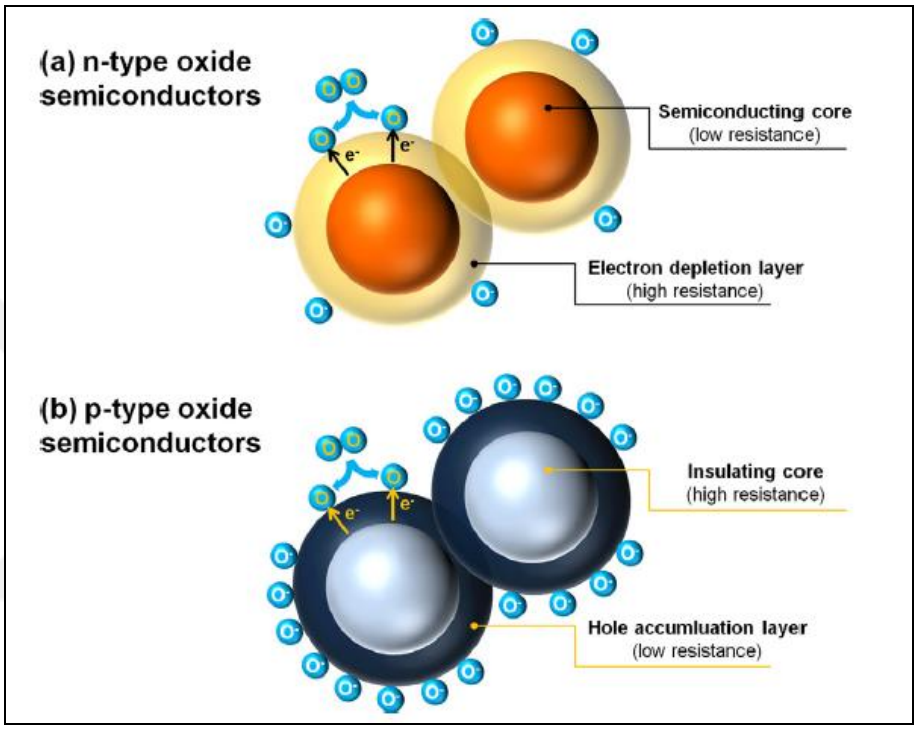

Figure 2.2: A schematic representation of conduction mechanism for a) n-type and b) p-type MOX.

The chemical reaction between oxygen ions and target gas molecule changes the carrier concentrations in the conductivity and thus, change of senor resistance. The change in sensor resistance depends on a type of MOXs. A general view on chemical reaction between target gas and oxygen ions is given in as;

$$X + O_{ads}^{b-} \xrightarrow{k_{gas}} X' + be^{-} \tag{2.4}$$

where X and X' is target gas and out gas, respectively. b is the number of electrons and k_{gas} is the reaction rate constant of gas reaction [21]. A rate equation for electron density can be written as

$$\frac{dn}{dt} = k_{gas}[O_{ads}]^b X^b \tag{2.5}$$

where n is the electron concentration under the gas atmosphere [21]. The k is the reaction rate constant described as;

$$k_{gas} = Aexp(-\frac{E_a}{k_b T}) \tag{2.6}$$

where E_a is the activation energy of a reaction, k_B Boltzmann constant and T is absolute temperature [21]. By using the equation (2.5) at an equilibrium state under gas ambient and air ambient and using the carrier concentration defined as n=α/R (where R is the resistance and α is a proportional constant) sensivity can be defined as;

$$S_g = \frac{R_a}{R_g} = \frac{\Gamma_t k_{gas}[O_{ads}^{ion}]^b [X]^b}{n_0} + 1 \tag{2.7}$$

A compact form of sensivity relation on gas concentration X can be written as;

$$S_g = aX^b + 1 \tag{2.8}$$

where a is a controllable parameter [21].

2.1.2.1. Surface to Volume Ratio

The surface-to-volume ratio is actually related with the surface activation. The increased surface area over volume cause more interactions between electrons in conduction band of MOX and O_2 molecules. This affects directly the density of the oxygen ions. The adsorbed oxygen ions can be written in terms of surface-to-volume ratio as;

$$[O]_{ads}^{ion} = \frac{\sigma_0 \Phi V_m}{V_s} \tag{2.9}$$

where σ_0 is a number of oxygen ions per unit area, Φ is a ratio of surface area per volume of material V_m and $V_s$is a system volume [21]. By inserting equation (2.9) onto equation (2.7) gives

$$S_g = \frac{\Gamma_t k_{gas} \left(\frac{\sigma_0 \Phi V_m}{V_s}\right)^b}{n_0} X^b + 1 \tag{2.10}$$

The proportional relation between surface-to-volume ratio and sensivity is clearly seen from the equation (2.10) [21].

2.1.2.2. Debye Length

The existence of surface-localized acceptor and donor states in semiconductors causes to charge transfer between bulk and surface in order to establish thermal equilibrium between the two [7]. A surface space charge region, a non-neutral region (with a non-zero electric field) in the semiconductor bulk, is created by charge transfer. Actually, the sensor resistance is caused by two reasons; the space charge region along the nanowire and band bending between the nanowires. According to the space charge model, L_d (Debye length), can be expressed by

$$L_d = \left(\frac{\varepsilon k_B T}{q^2 n}\right)^{1/2} \tag{2.11}$$

where ε is a static dielectric constant, q is an electrical charge of a carrier, and n is a carrier concentration. It can be seen that the Debye length depends only on the carrier concentration at a constant temperature T [21].

In this model, geometric shape of nanowire is taken as a cylinder, a conductive channel is assumed to be along the axis of the cylinder. It can be considered as the conductive channel is reduced or increased along the radial direction of cylinder with a thickness of L_d. The carrier concentrations can be described in terms of Debye length and D diameter of cylinder as;

$$n' = n_0 \frac{\pi(D - 2L_d)^2}{\pi D^2} \tag{2.12}$$

where n_0 is the carrier concentration of intrinsic material and n' is carrier concentration of the Debye length [21]. The effect of depletion layer on sensivity of MOX nanowires can be obtained by inserting equation (2.12) in equation (2.10)

$$S_{L_d} = \left(\frac{\Gamma_t k_{gas} \left(\sigma_0 \Phi \left(\frac{V_m}{V_s} \right) \right)^b}{n_0} \right) \frac{D^2 X^b}{(D - 2L_d)^2} + 1 \tag{2.13}$$

This formula shows the dependency of sensivity on diameter of diameters of nanowires (D) and Debye length (L_d) [21]. Three conditions decide which mechanism has dominant effect on sensivity, Depletion layers on nanowires or potential barrier of contacts between nanowires [21]. In condition of D >> 2w (depletion layer width), the potential barriers of the contacts between wires has importance on sensing mechanism [21]. The sensivity is independent of the diameter of nanowires D. In condition of D > 2w condition exists, the sensivity is affected by both diameter of nanowires and the potential barrier [21]. In condition of D ≤ 2w, the sensor resistance is controlled only by the surface depletion [21].

2.2. Cupric Oxide (CuO) and Cuprous Oxide (Cu_2O)

Copper oxides have two oxidation phases; cuprous oxide (Cu_2O) and cupric oxide (CuO). They are p-type metal oxide semiconductors and their band gap energies are relatively narrow, for Cu_2O~1.2 eV and CuO~2.1 eV. They are potentially photovoltaic materials that because of their low-cost, earth abundance and non-toxicity. Nanostructured Cu_xO materials are great candidates for gas sensor applications because of their high absorption coefficients, remarkable catalytic effects, and optoelectronic properties.

Various synthesis methods have been studied on cuprous oxide(C_2O) nanostructures such as thermal oxidation, hydrothermal [22,23], electrodeposition [24], template assisted [25], RF magnetron sputtering, plasma reduction [26]. Among these synthesis methods electrochemical method had a special significance for

scientists because direct synthesis of Cu_2O nanostructures have been complex and needed some extra processes. Although Cu_2O was prone to peeling off Cu substrate during anodization, the intermediate products, such as $Cu(OH)_2$ or CuCl, can stay tightly on the surface of anode after anodization [27]. In order to convert intermediate products to CuO and Cu_2O nanostructures, Z. Zhang et al. used three methods H_2O_2 hydrolysis, thermal reduction in H_2 gas and Fehling method[28]. Wu et al. used thermal annealing under N_2 gas flow [29]. Allam and Grimes offered RTC infrared furnace annealing under air ambition and vacuum annealing [30]. In this work, vacuum annealing was used to synthesis after electrochemical process.

There are also many synthesis methods for the synthesis of CuO nanostructures in literature. The huge parts of these studies were based on hydrothermal and solvothermal methods to get single phase of CuO nanostructures [31]. However, it seems a problematic usage for gas sensors because of the powder form of synthesized products. On the other hand, the thermal oxidation method has been extensively studied for the direct synthesis of CuO nanowires on Cu plates and Cu films substrates [32,33]. Actually, there have been many reports on cracking problems because of the high surface tension of Cu films on substrates. The high surface tension of Cu film also cause to peeling off from substrates. Wang et al. offered Ti metal films to handle this adhesion problem between Cu films and substrates [34]. In this work, the thermal oxidation method was used to synthesize CuO nanowires on Si substrates with Ti interlayer film.

There are extensive researches on gas sensor applications based Cu_xO nanostructures. The remarkable photo-catalytic property of Cu_2O provided it to take place in sustainable, safe production of H_2 with water-splitting [35] and sensor applications. Although there are many studies on gas sensing properties of CuO, there are limited studies on gas sensing properties of Cu_2O. J. Zhang et al. compared alcohol, gas oil and H_2S sensing of CuO and Cu_2O nanospheres [36]. H. Zhang et al. showed the ethanol sensing of Cu_2O hierarchical hollow microspheres, nanocrystallites and solid microspheres [37]. Gasparatto et al. compared both H_2 production and sensing properties of CuO and Cu_2O nanodeposits on Al_2O_3 substrates [38]. Guan et al. synthesized Cu_2O nanorods and investigated ethanol sensing properties of them [39]. Lastly, Zolfaakar et al. compared ethanol sensing properties of CuO and Cu_2O nanoparticles [40].

2.3. Organics Based Conductometric Gas Sensors

Another sensitive layer used for gas sensors are some organic materials having semiconducting properties. Conductive polymers (CP) and metallophthalocyanines (MPc) are attractive features for gas sensors such as; great processability, stability and rich substitution chemistry [41]. In addition, they are extremely sensitive to some gases and their gas sensing properties have been studied for twenty years [42-44].

The conductive polymers have been preferred for gas sensors because of their promising features such as; the easy and cheap synthesis methods and adjustable physical and chemical properties by introducing different substituents, or copolymerizing with different monomers, mechanical flexibility, ease of processing, modifiable electrical conductivity and a lower power and require simpler electronic setups [45-50]. Famous conducting polymers in literature for gas sensing applications are polythiophene and its derivatives [51,52], polypyrroles [53,54], polyaniline and their composites [51,55-57]. The insulating polymers such as polyacrylaonitrile (PAN), polysterene and polycarbonates etc. have become electrically conducting with electropolymerization of polyacrylaonitrile, polythiophene, polypyyrole and some composties of them [58,59]. These polymers show sensor response proportional to analyte gas concentration and rapid adsorption/desorption kinetics [60].

Phthalocyanines were other organic sensitive materials for gas sensors applications. Actually, they have been used as dye and pigment agents during a long period. They have been also used in nonlinear optic applications and gas sensors with their electroative behavior produced with the incorporation of a transition metal on its structure, metallophthalocyanines [61-63]. Phthalocyanines are composed by four pyrrole ring are used for the addition of substituted groups [64,65]. A schematic structure of phthalocyanine structure is shown at figure 3. Phthalocyanines can detect the O_3(ozone) [66], NO_2 [67-69], VOCs [70,71], halogens (Cl_2, Br_2,) [72] gases.

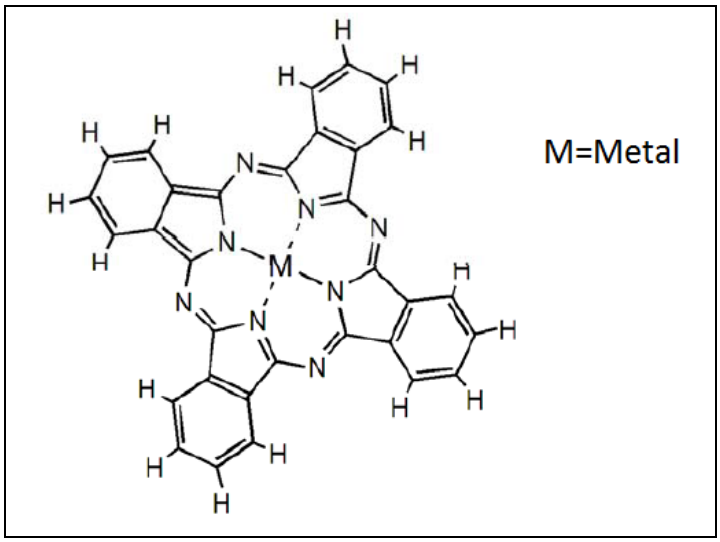

Figure 2.3: A schematic representation of phthalocyanine.

3. EXPERIMENTAL METHODS

3.1. Fabrication of Cu_2O Nanowires

3.1.1. Cu Thin Film Coatings

The selection of substrates is an important process for sensor device. Three different substrates were tested in Cu thin film coatings. The microscope glasses, Si wafers and Al_2O_3 were cut in 10x10x1mm dimensions and used as substrates for Cu_2O nanowires synthesis with anodic oxidation. The substrates were etched and cleaned with 1:5 H_2SO_4 aqueous solution acetone, ethanol and deionized water in an ultrasonic bath for 5 minutes. Etching process was added the process after some observations on coatings to increase the adhesion between glass and Cu film. Cu thin films of 100 nm, 450 nm, 1µ and 2µ thicknesses were evaporated on pre-cleaned substrates in a Leybold Univex 450 coater system.

3.1.2. Anodic Oxidation

Cu film was anodized in 0,2 M KOH + 0,1 M NH_4F aqueous solution in a thermo-stated bath using a dc power supply, a platinum foil as a cathode and Cu thin film on glass substrate as an anode. A shematic representation of experimental set-up is given at figure 3.1.

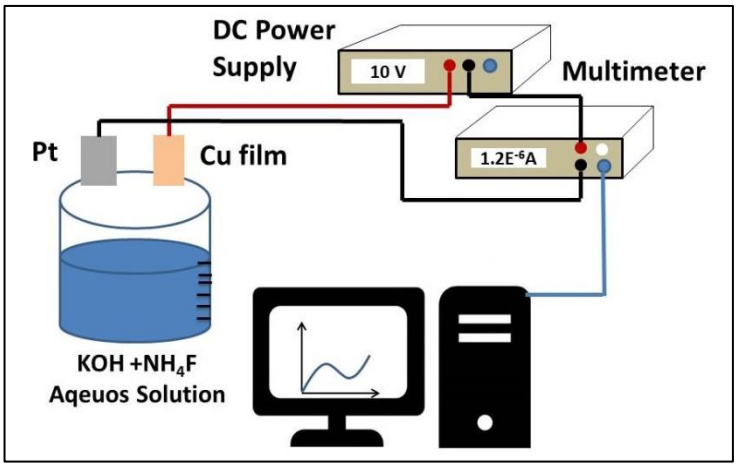

Figure 3.1: Schematic representation of anodic oxidation experimental set-up.

The temperature, anodization voltage and time values are listed at table 3.1.

Table: 3.1. Anodization Parameters

Anodization Voltage(V)	Anodization Temperature (^{o}C)	Anodization Time (seconds)
4 V	23 °C	300 sec
6 V	23 °C	8 sec
6 V	23 °C	300 sec
10 V	23 °C	300 sec

After anodization, samples were rinsed in deionized water, dried with N_2 gas and annealed at different temperatures and ambiences. The anodized sample for 300 seconds at 10 V is annealed at 300 °C in tube furnace for 1 hour in room atmosphere, under dry air flow, low (10^{-2} bar) and high vacuum(10^{-5} bar) conditions.
The low vacuum was set up with 1 L test chamber using mechanical pump (Leybold L408).

3.2. Fabrication of CuO Nanowires

3.2.1. Cu Thin Film Coatings

Cu films were coated on Si substrates (10x10x1 mm) with Vaksis Midas RF Magnetron Sputtering System. The Si substrates were wet-cleaned by acetone and de-ionized water followed by baking at 100 ºC for 10 min to evacuate moisture. A 30-nm-thick Ti layer was firstly deposited to serve as the adhesion layer and then 1 µ Cu film was coated by RF sputtering. The targets used to deposit Ti layer and Cu were 99.99% pure. The distance between the target and the sample was at 7 cm. The Ar flow rate, base pressure, working pressure and substrate temperature were maintained same for sputtering at 50 sccm, 5 × 10−6 Torr, 5 mTorr and 25 ºC, respectively. RF power was set 80 W for Ti target and 120 W for Cu target.

3.2.2. Thermal Oxidation of Ti-Cu Films

The Ti-Cu films on Si substrates were thermally oxidized in tube furnace at different temperatures to find the optimum values for CuO nanowires synthesis. The each sample was oxidized at 350 °C, 400 °C, 450 °C and 500 °C one by one for 4 hours.

3.3. Synthesis of Hybrid Structures

The organics were coated on the nanostructured CuO and Cu_2O nanowires with spin coating method. Firstly, the Cu-Pc (Copper- Phthalocyanine) solution is prepared by solving 10 mg Cu-Pc in 10 ml Toluene. The P(S-*co*-CMS-C_{60}) (fullerene functionalized poly(styrene-co-chloromethylstyrene)) solution is prepared by solving 1 mg P(S-*co*-CMS-C_{60}) in 10 ml Tolune. Then the solutions were coated by spin coater at 1000 rpm onto the CuO and Cu_2O nanowires.

3.4. Fabrication of Gas Sensor Device

In order to investigate DC electrical and gas sensing measurements of samples, we evaporated gold (Au) interdigital electrodes (IDT) onto samples with Leybold Univex 450 coater system by using a shadow mask. The Au IDT has 10 fingers which have 100μ widths, 5 mm lengths and 100 nm thicknesses.

3.5. Gas Measurement System

The CuO nanowires, Cu_2O nanowires, P(S-*co*-CMS-C_{60})@CuO hybrid, Zn-Pc@Cu_2O hybrid and P(S-*co*-CMS-C_{60})@Cu_2O hybrid gas sensors were tested against to different concentrations of H_2 and Ethanol gas under dry air flow in Gebze Technical University (GTU) Sensor Laboratory and against to different concentrations of NO_2 gas under dry and humid air flows in Barcelona University Nanoelectronics Laboratory.

During the H_2 and Ethanol measurements, the temperature of the sensor devices was controlled with a Lakeshore 340 temperature controller in order to measure temperature dependent sensor parameters. The DC electrical measurements of Cu_2O nanowires were done under 200 sccm high purity dry air flow in the temperature range between 303 – 473 K. Keithley 6517A Electrometer/High Resistance Meter was used for I-V measurements with a sweep rate of 50 mV/s between -1V and +1V in a homemade test chamber (1L). Then, the samples were heated up to 473 K under 200 sccm high purity dry air flow and waited for 30 minutes to get steady state. Concentrations were controlled by using multi gas controller (647C MKS Instruments) and gas flow meters for sensor measurements. A constant bias voltage was applied to sensor devices and the dc current of them was measured with a Keithley 6517A Electrometer/High Resistance Meter. The DC current was monitored continuously under dry air flow to establish the baseline of the device and different concentrations of gases were exposed into the test chamber at desired temperatures. Then the chamber was cleaned with dry air. A schematic representation of gas measurement system is given at figure 3.2.

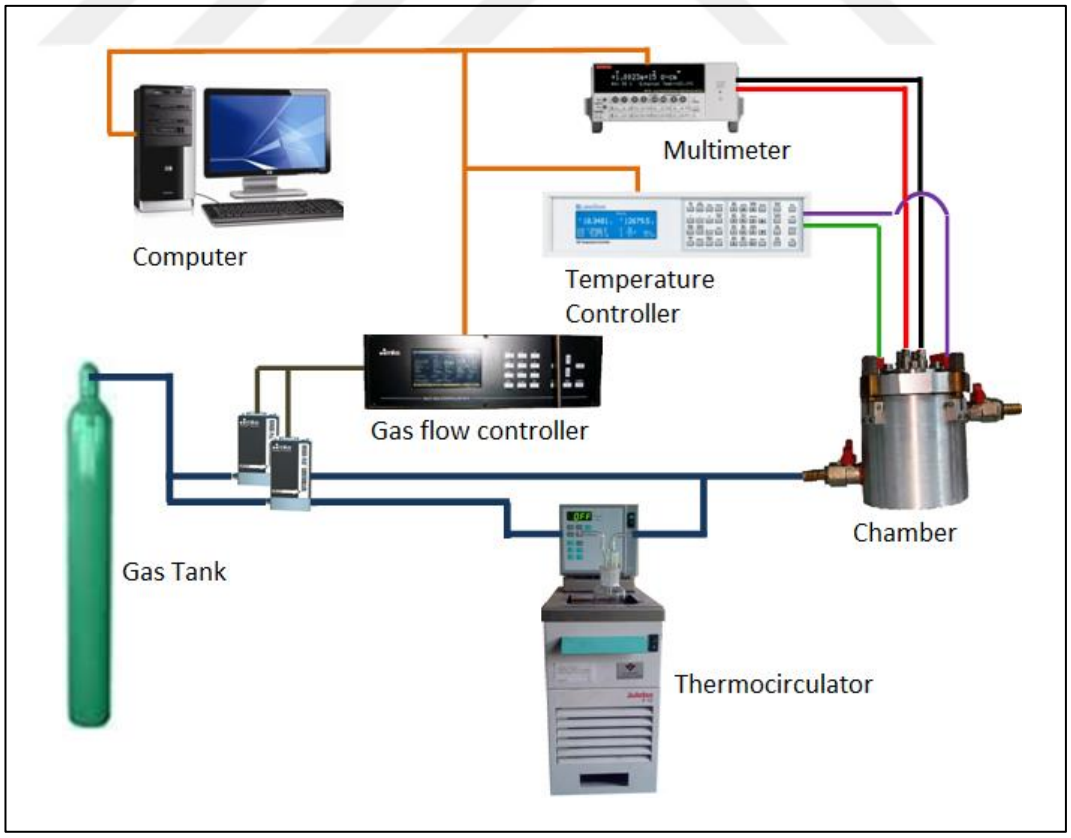

Figure 3.2: A schematic representation of gas measurement system.

For the NO_2 measurements, temperature of sensor devices was controlled by applying a constant voltage on Ni-Cr wire. The DC current changes with time under 1V potential were recorded for all samples. We used two Keithley 2400 sourcemeters for electrical measurements and Bronkhorst gas flowmeters to control flows in set up.

The sensor responses of this work were calculated with using relation;

$$R_{sensor}(Sensor\ Response) = \left(\frac{|\Delta I|}{I_g}\right) \tag{3.1}$$

where ΔI is the change in the current when exposed to analyte gas and I_g is the minimum value of the devices when exposed to analyte gas.

4. RESULTS and DISCUSSIONS

4.1. Cu_2O Nanowires

4.1.1. Anodic Oxidation

The Cu films on glass substrates did not peel off from the surface in the solution. Current density vs time for anodized Cu thin film with a constant anodization voltage of 10 V at anodization temperature of 23 °C during anodization process is shown in figure 4.1.

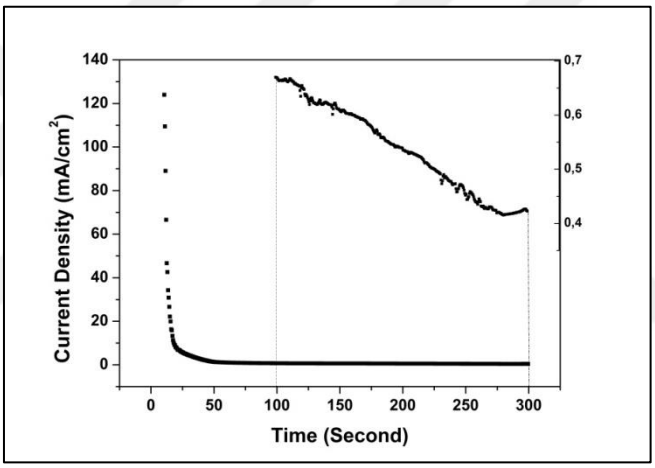

Figure 4.1: Current density vs time graph of Cu thin film.

The current density decreases sharply and come in from 127 mA/cm^2 to steady state 0,8 mA/cm^2. Copper dissolution, formation of copper hydroxides and copper oxides took place in anodization process. A possible formation mechanism of copper oxide and hydroxide species;

$$Cu + 2OH^- \rightarrow Cu_2O + 2e^- + H_2O \qquad (4.1)$$

Allam and Grimes reported that the oxygen reduction may occur at the counter electrode under OCP. They observed an slight increase in current density with time and explained with the transformation of dissolving pits into pores on oxide film [30]. However, it is not observed such an increase in current density with time in

this study. The difference between thicknesses of Cu foil and Cu film could be effective on the pore formation. The lower thickness of Cu film might have prevented the pore formation and increase in current density [73].

4.1.2. Structural Characterization of Cu_2O nanowires

In order to investigate the formation process and surface morphology of substrates, SEM analyzes were done by scanning electron microscopy (SEM, Philips XL 30S). The sample anodized at 6V for 8 seconds (figure 4.2.a) showed the start of wire formation after the formation of hydroxide layer. We characterized the shape of nanostructures anodized in 0,2M KOH+ 0,1M NH_4F soluiton at 23 ºC with SEM at different voltages 4V (figure 4.2.b), 6V (figure 4.2.c), 10V (figure 4.2.d). The increasing voltage led to formation of thinner and denser nanowires.

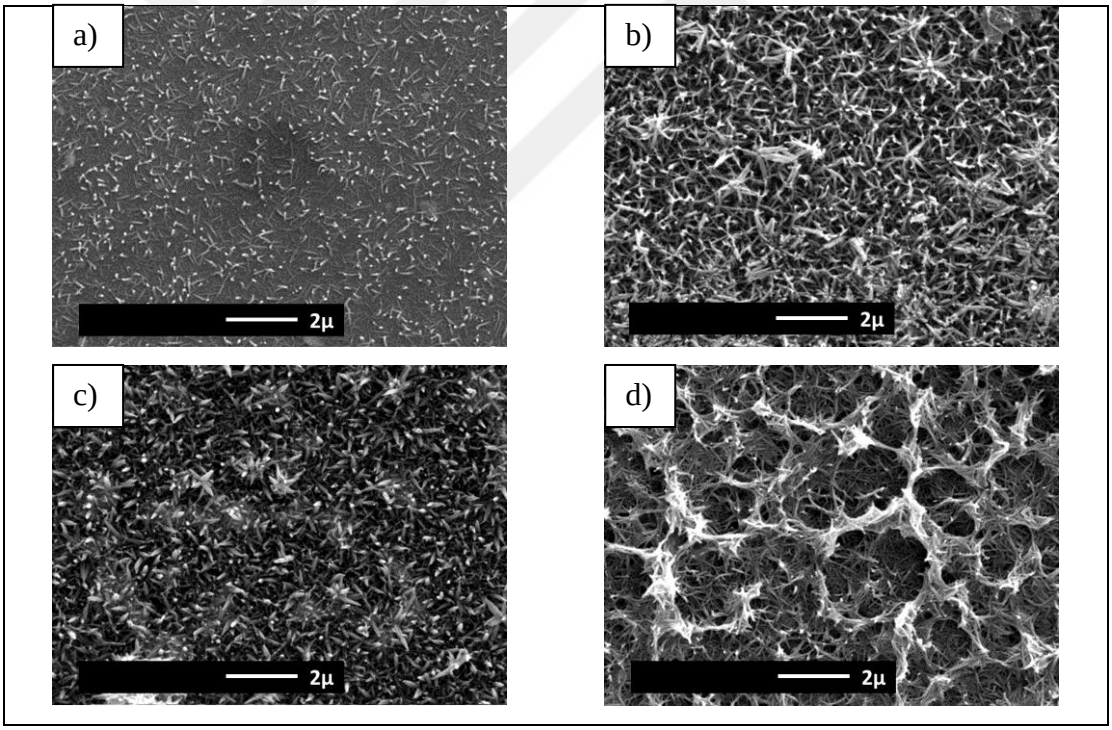

Figure 4.2: SEM images of copper oxide nanowires after anodization a) 6V 8 sec. b) 6 V 300 sec c) 4 V 300 sec. d) 10 V 300 sec.

The XRD pattern of as-synthesized sample (figure 4.3.a) observed only peaks at 2θ values of 43.6° and 50.8° corresponding to Cu (111) and (200) planes, which revealed that the nanowires were amorphous. In order to get dehydration of hydroxides and crystal formation the samples were thermally annealed. Atmosphere,

high and low vacuum conditions were tested for annealing process. In the atmosphere, the wire formation was broken down or distorted because of the high surface tension of Cu film on glass and weak amorphous structures of nanowires. For the protection of nanowires, thermal annealing was done under low vacuum. After vacuum annealing the patterns (figure 4.3.b) showed the Cu_2O (111) plane peak at 36.4° [74] and decreased Cu peak counts at 43.6° and 50.8°.

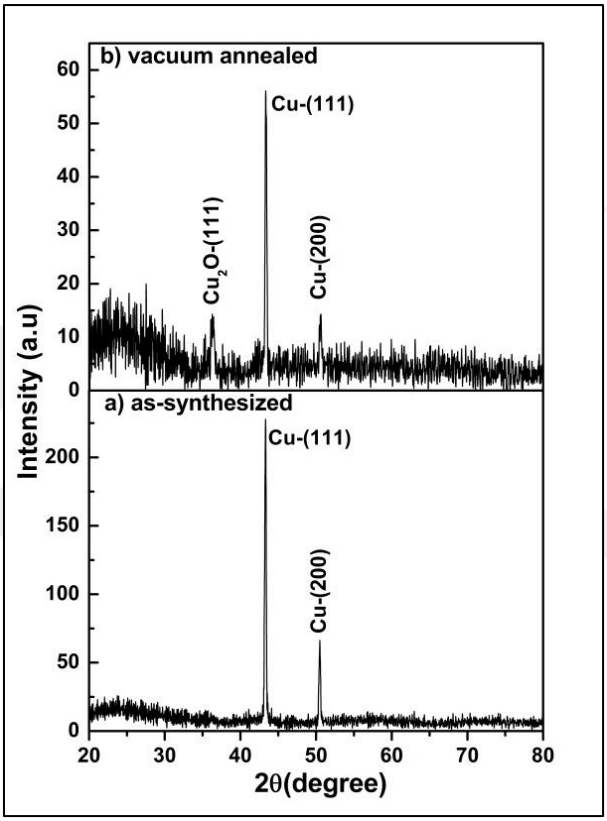

Figure 4.3: XRD patterns of a) as-synthesized sample b) vacuum annealed sample.

The XPS measurements of samples were done to get more information about the structure and composition of the nanowires. Figure 5 shows the XPS spectra the (a) Cu 2p and (b) O 1s core levels for as synthesized and annealed samples.

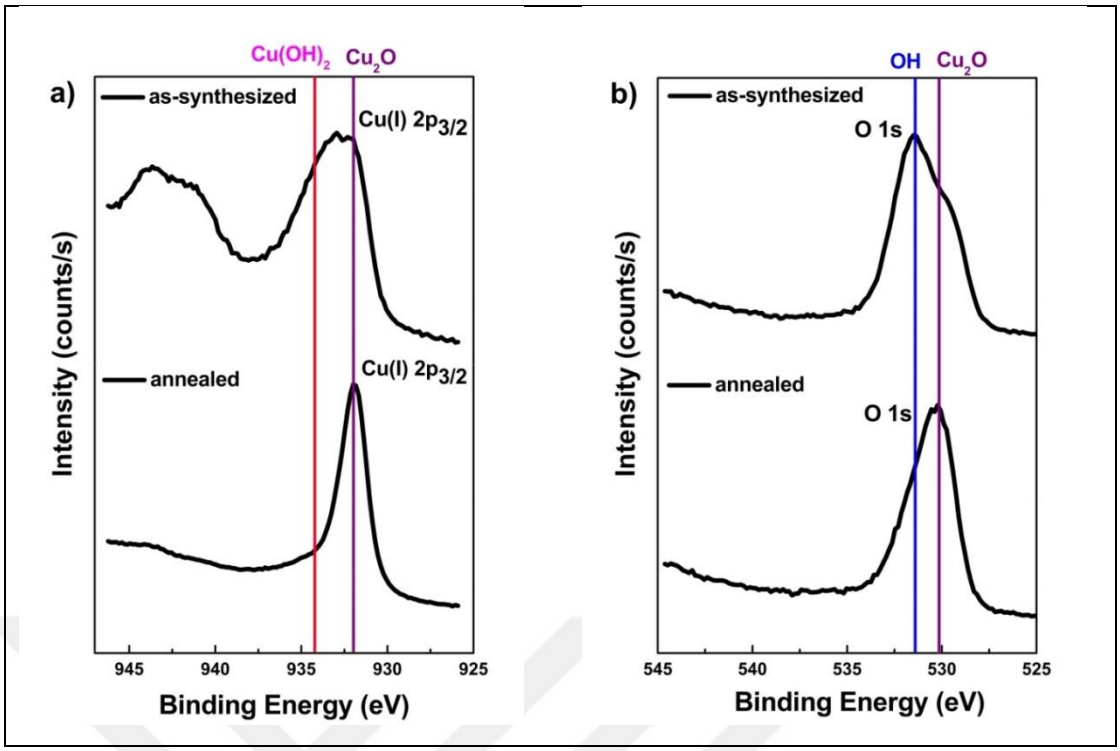

Figure 4.4: XPS results of annealed and as-synthesized samples a) Cu 2p peaks b) O 1s peaks.

As shown in figure 4.4.a, the Cu 2p peaks at the binding energies of 932.4 eV and 934.1 eV are corresponded to that of Cu+ in Cu_2O and $Cu+^2$ in $Cu(OH)_2$ respectively.. The peak position of Cu+ in Cu_2O is reported between 932.0 - 932.7 eV [27,30,75-82] and it is well agreement with our results. The XPS peak of $Cu(OH)_2$ at 934.1 eV is disappeared after annealing at 280 ºC in vacuum for 15 minutes as seen in figure 4.4.a. On the other hand, the peak position of Cu (between 932.2 - 933.1 eV) is near to Cu+ in Cu_2O and cannot be definitely discerned from each other by only analyzing Cu 2p core XPS spectra. However, the O 1s peaks at 530.1 eV and at 531.5 eV correspond to O_2- ions in Cu_2O and surface-adsorbed oxygen species (O_2 or OH), respectively. As a result, XRD and XPS measurements all prove that Cu_2O is the only product.

4.1.3. Optical Characterization of Cu_2O nanowires

The results of UV-vis absorption (figure 4.5.a) showed that annealed sample have stronger lighter absorption ability then as-synthesized sample. The UV-vis absorption data was used to determinate the optical band gap and the type band to

band transition of Cu_2O annealed sample. We plotted the $(\alpha h\nu)^2$ versus $h\nu$ in figure 6.b for direct transition and the $(\alpha h\nu)^{1/2}$. The optical band gap was found 2.24 eV for Cu^2O nanowires from the slope of $(\alpha h\nu)^2$ versus $h\nu$ graph.

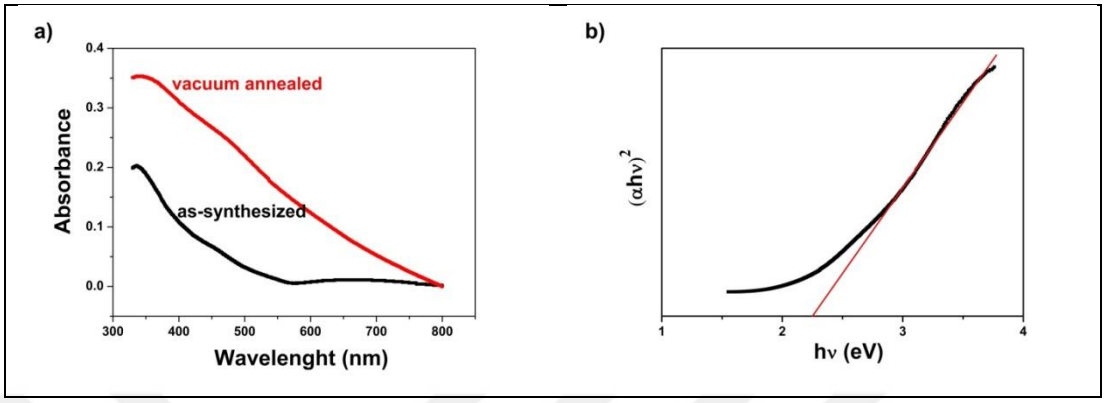

Figure 4.5: UV–vis analysis results of Cu_2O nanowires a) UV–vis absorbance of Cu_2O and as-synthesized sample, b) plot of $(\alpha h\nu)^2$ versus $h\nu$.

Singh et al. showed a similar absorbance graph of Cu_2O nanowires and estimated the optical band gap of Cu_2O nanowires 2.67 eV. They stated that the higher band gap can be attributed to the quantum size effect of Cu_2O nanowires [83]. In this work, there is amorphous thin copper oxide thin film under the Cu_2O nanowires. This copper oxide thin layer might have reduced the quantum size effect on optical band gap.

4.1.4. Electrical Characterization of Cu_2O nanowires

The I-V curves at different temperatures of Cu_2O nanowires were plotted in figure 4.6.a to illustrate an increase in conductivity with temperature. The Ohmic behavior as shown by the I-V curves is due to the contact of Au electrode and Cu_2O nanowires [84,85]. In order to investigate the thermal conduction mechanism of Cu_2O nanowires we used the relation:

$$\sigma_{DC}=\sigma_{o}.\exp(\frac{-Ea}{kT}) \quad (4.1)$$

where Ea is activation energy, T temperature, k Boltzmann's constant and σ_o proportionality constant. Figure 4.6.b shows the semi-logarithmic graph of

conductivity at 1V vs reciprocal temperature for the Cu_2O nanowire exposed to dry air. The activation energy of Cu_2O nanowires was determined 0.63 eV by plotting ln(σ) vs 1000/T graph in figure 4.6.b. The activation energy is smaller than the optical band gap energy which may indicate the conduction is due to the transition of charge carriers from valance band to acceptor level.

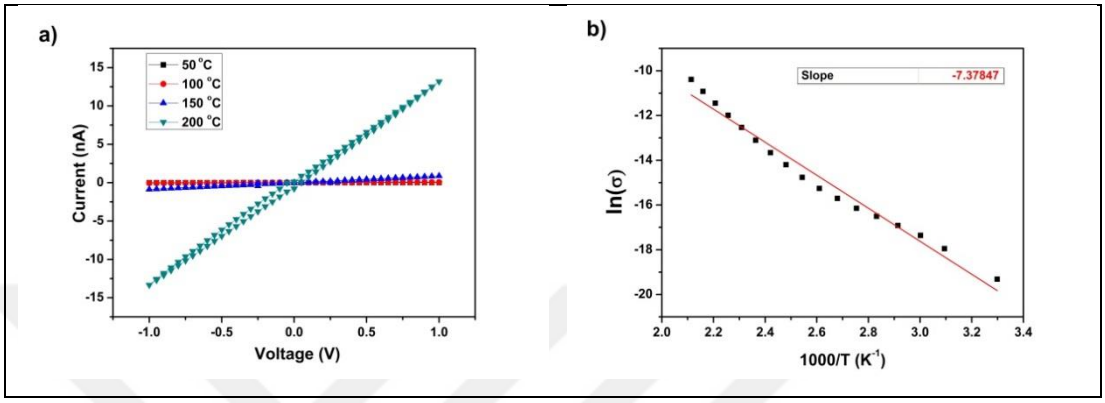

Figure 4.6: a) I-V characteristics of Cu_2O nanowires b) The dependence of logarithmic current, ln I, on the inverse of the temperature, 1000/T.

4.1.5. Gas Measurements

Cu_2O nanowires were used for H_2 sensing measurements. 1000 ppm, 500 ppm and 250 ppm of H_2 was exposed to the devices at 200 ºC, and after ~10 min waiting the chamber was cleaned with 200 sccm high purity dry air flow for ~30 min. Figure 4.7 shows the sensor response of sample to 250 ppm, 500 ppm and 1000 ppm H_2 gas flow at 200 ºC. The results showed that the sensor responses had proportionality according to ppm values and also the recovery of sample was successful.

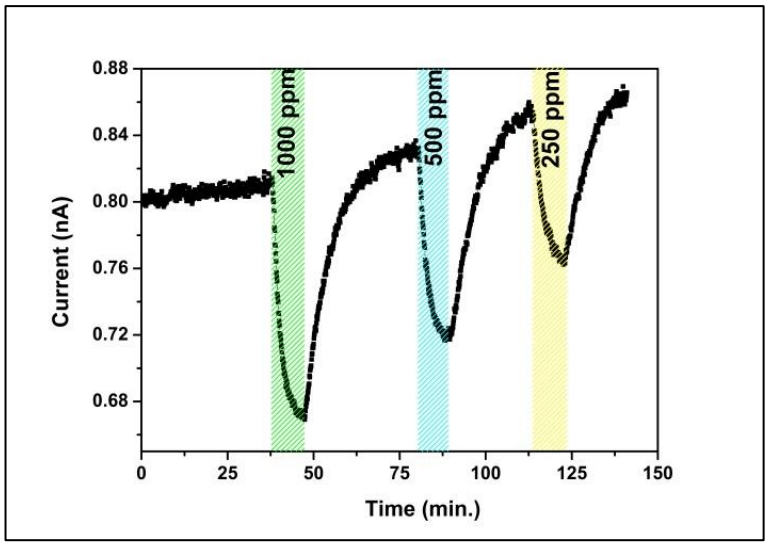

Figure 4.7: Sensor results of Cu_2O nanowires at 200 ºC to 1000, 500, 250 ppm H_2 gas.

In order to determine the optimal operating temperature for Cu_2O nanowires to H_2 gas, they were exposed to 1000 ppm H_2 at various operating temperatures of 150 °C, 200 °C and 250 ºC. Figure 4.8 shows the sensor response of sample at 250 ºC to 1000 ppm H_2 gas and the comparison of sensor responses at different temperatures.

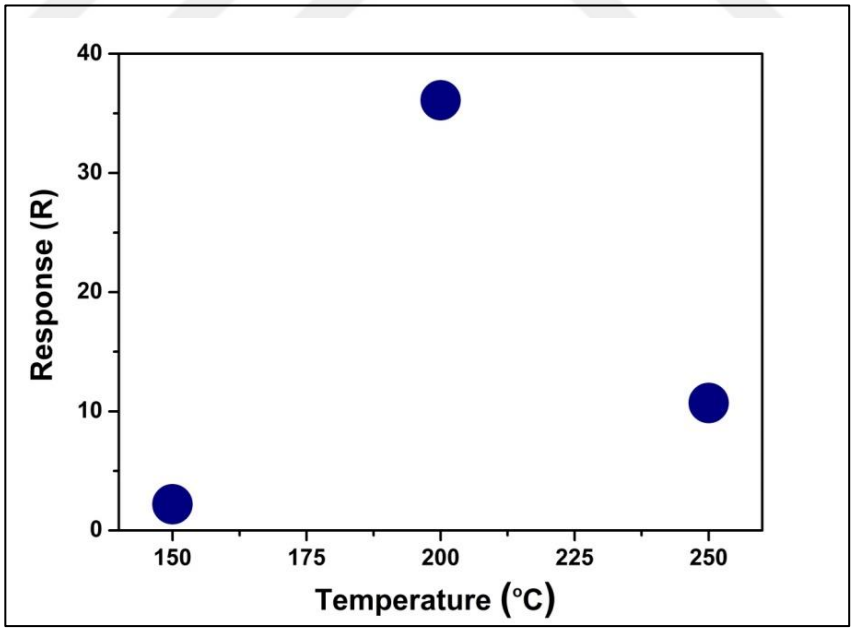

Figure 4.8: Sensor responses of sample at 150 °C, 200 °C and 250 ºC to 1000 ppm H_2.

Cu_2O nanowires also tested against 500 ppb, 1 ppm, 2.5 ppm and 5 ppm concentrations of NO_2 gas at 23 °C, 50 °C, 100 °C and 150 °C. Figure 4.9. shows the

sensor response of Cu_2O nanowires against different concentrations of NO_2 gas at 23 °C (figure 4.9.a.) and 50 °C (figure 4.9.b) under dry air flow.

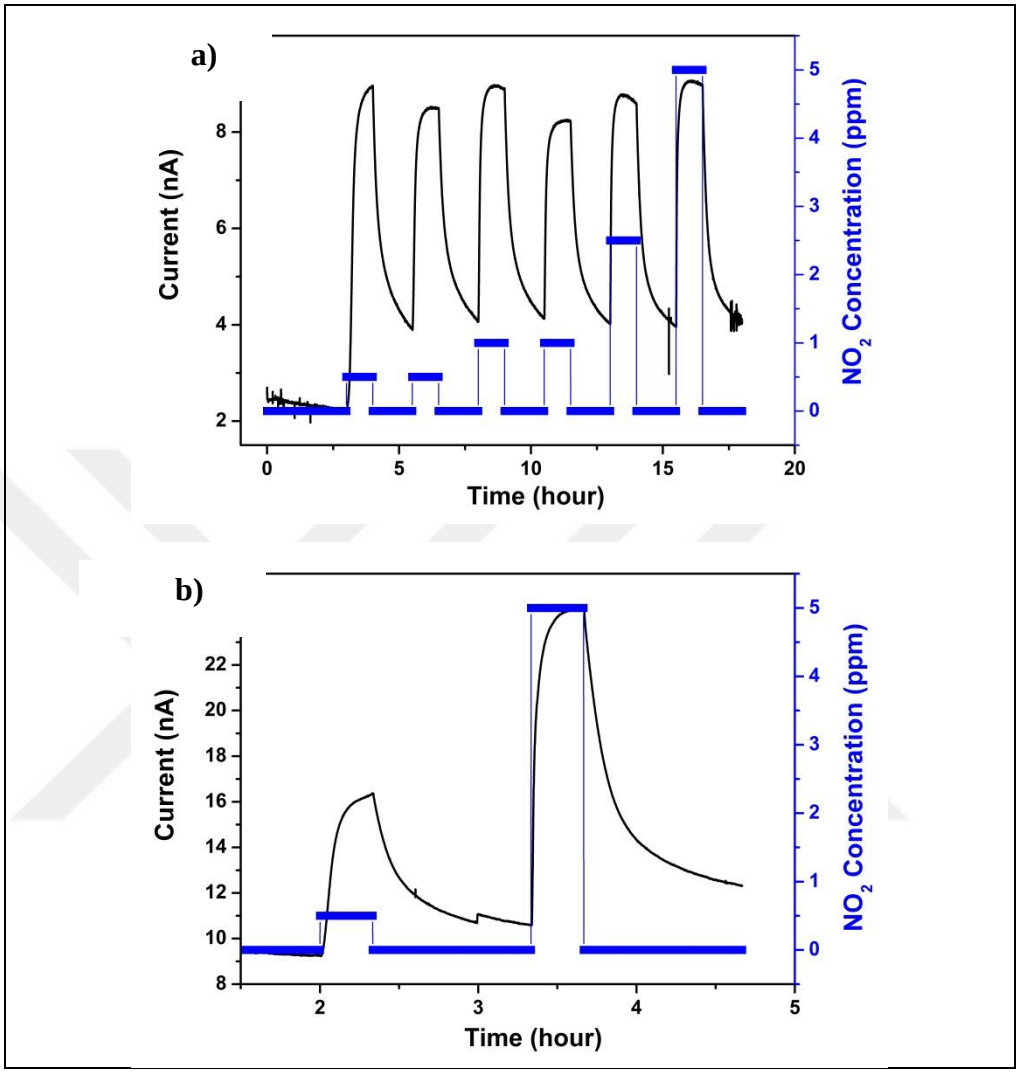

Figure 4.9: Cu_2O nanowires sensor responses at a) 23 °C b) 50 °C for different NO_2 concentrations.

While the response of sensor at 23 °C is the nearly same for all different concentrations, at 50 °C there is a considerable difference between sensor responses against 500 ppb and 5 ppm NO_2 concentrations. This shows the relation between the temperature and activation of surface states.

At the higher temperatures, the sensivity against NO_2 gas is increased. Figure 4.10 shows the sensor responses of Cu_2O nanowires at 100 °C and 150 °C against different concentration of NO_2 gas.

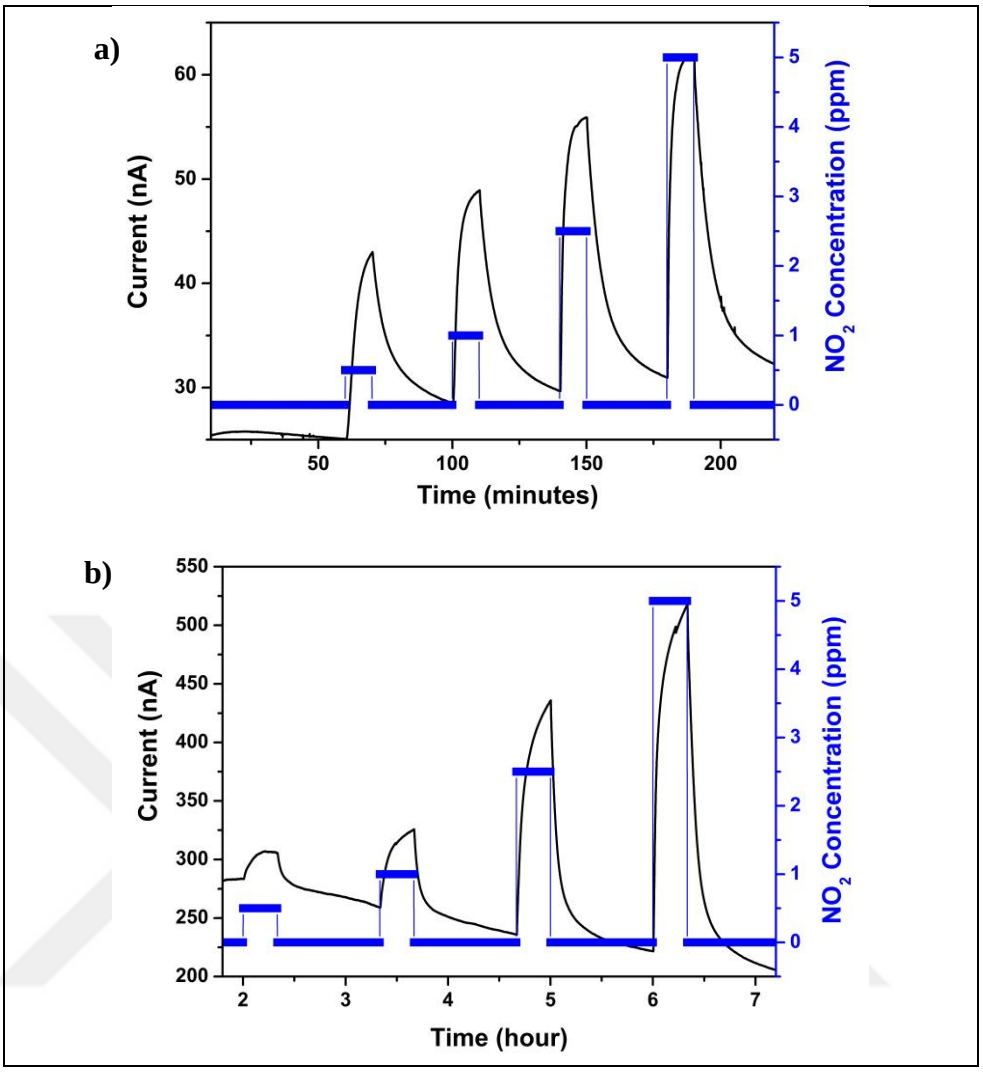

Figure 4.10: Cu_2O nanowires sensor responses at a) 100 °C b) 150 °C for different NO_2 concentrations.

To understand the effect of humidity on sensing, some measurements were also taken under humid air flow. The Cu_2O nanowires were tested against different concentrations of NO_2 gas under %38 humid air flow at 150 °C. (figure 4.11.a.) Cu_2O nanowires showed better NO_2 sensing under humid air. The comparison between the NO_2 sensor responses of Cu_2O nanowires under dry air and humid air flow against 0.5 ppm, 1 ppm and 5 ppm NO_2 concentrations is given below at figure 4.11.b.

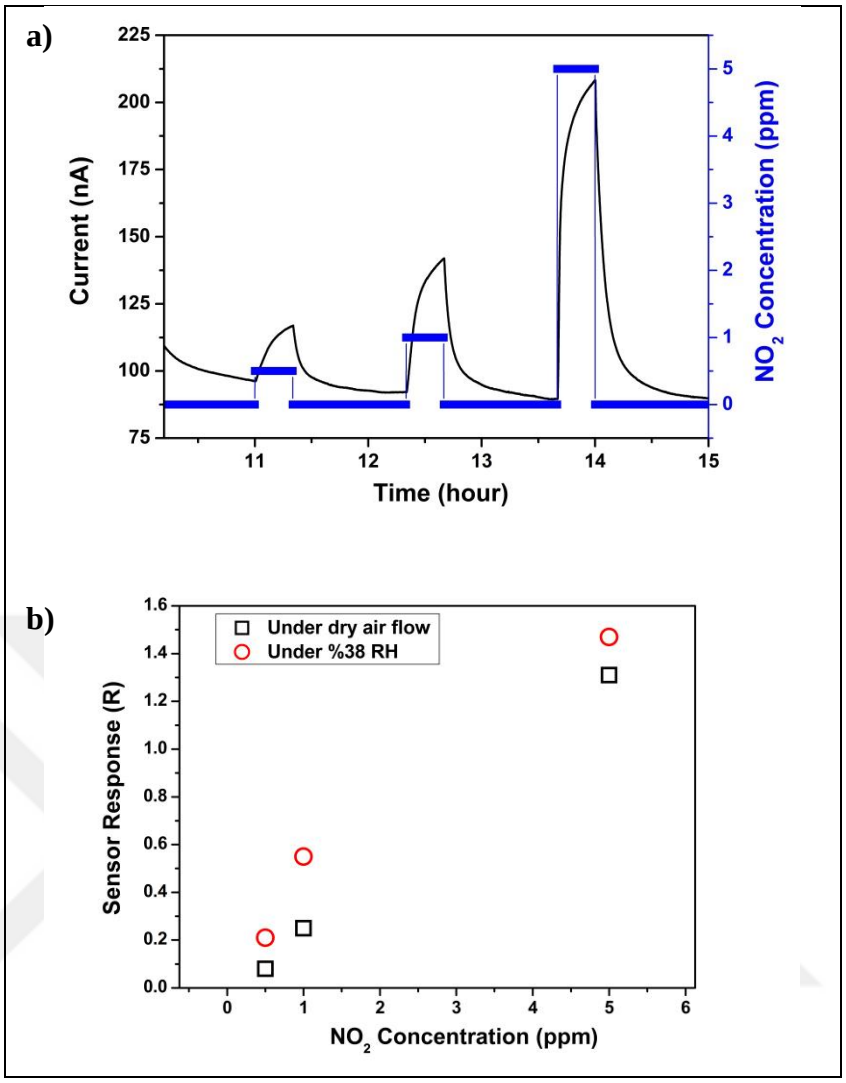

Figure 4.11. a) Sensor responses of Cu_2O nanowires against different NO_2 gas concentration at 150 °C under 38% RH. b) Comparison of sensor responses of Cu_2O nanowires under dry and humid air.

4.2. CuO Nanowires

4.2.1. Structural Characterization of CuO Nanowires

The characterization of CuO nanowires was done with SEM images and XRD measurements. According to SEM images (figure 4.12.) of thermally oxidized samples at 350 °C, 400 °C, 450 °C and 500 °C, the best homogeneity of CuO nanowires was observed in sample oxidized at 400 °C.

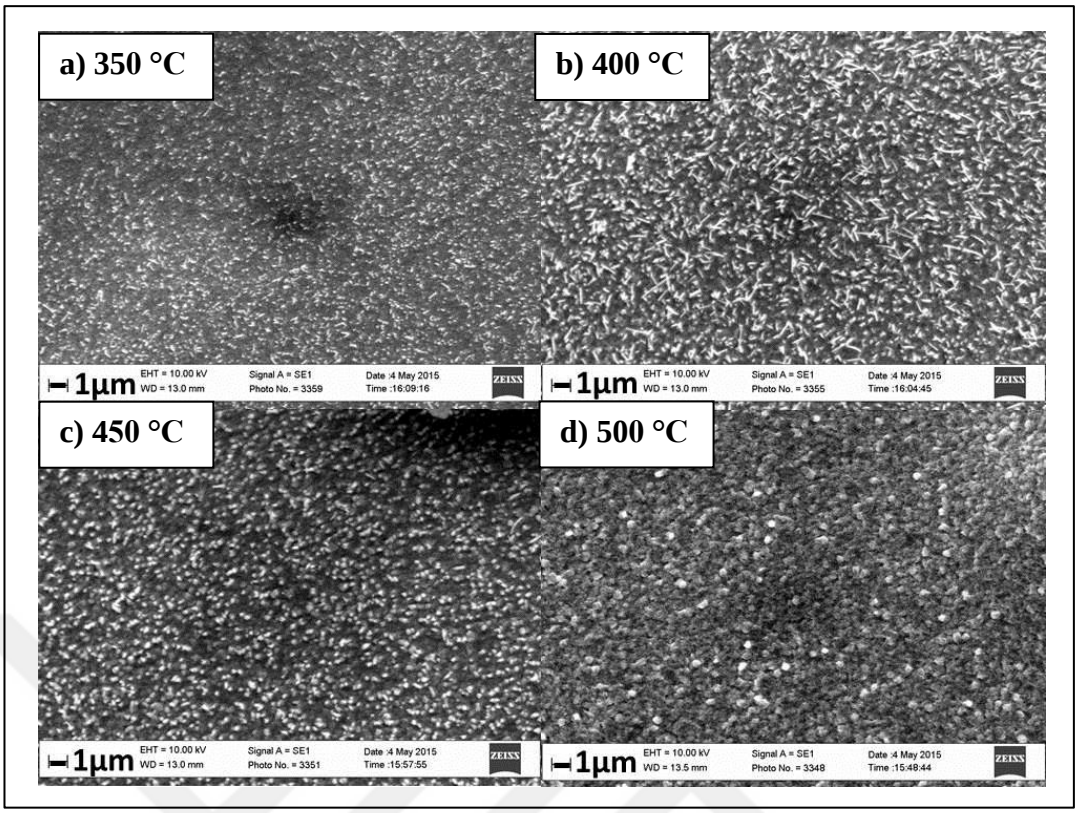

Figure 4.12: SEM images of CuO films oxidized at a) 300 °C, b) 400 °C, c) 450 °C and d) 500 °C.

The crystal structure of samples also investigated with XRD measurements. The patterns (figure 4.13) showed that there are not only CuO plane peaks but also Cu_2O plane peaks. The reason is that there is a Cu_2O layer at the bottom of CuO layer as a result of CuO nanowire formation. The formation mechanism of CuO nanowires is explained by the relaxation of compressive stress and by grain-boundary diffusion of Cu ions through the Cu_2O layer by researchers [86-90].

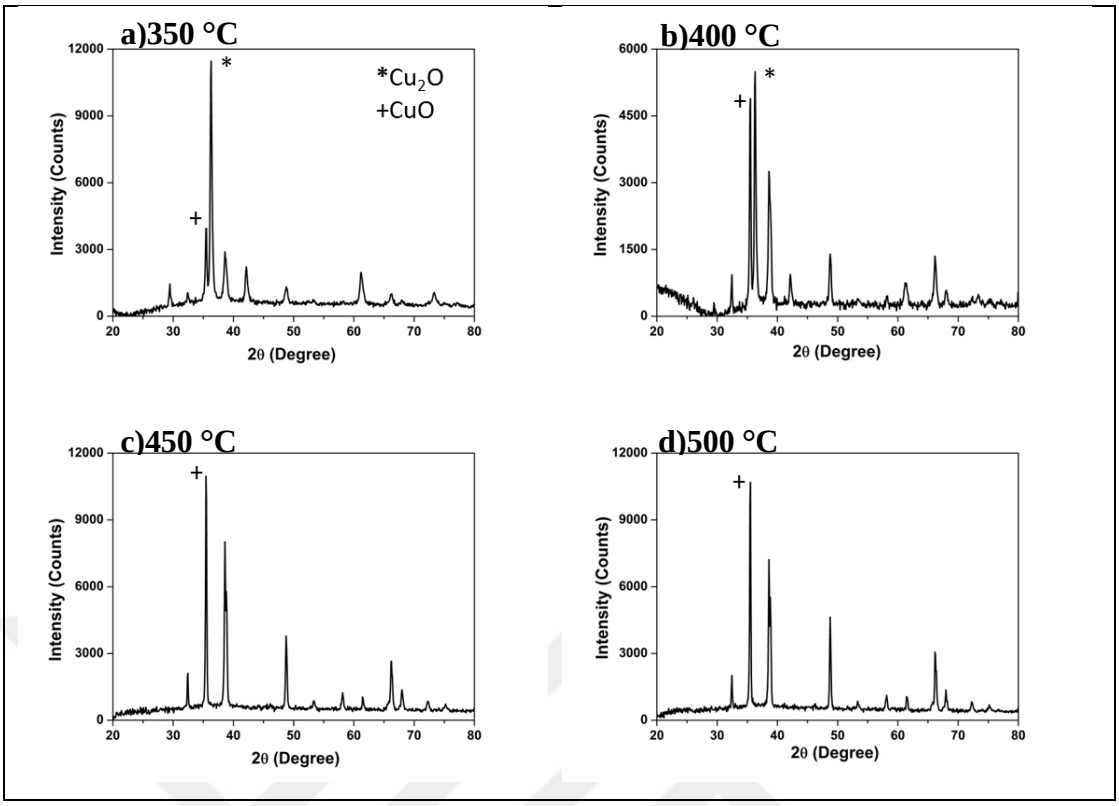

Figure 4.13: XRD patterns of annealed samples at a) 350 °C, b) 400 °C, c) 450 °C and d) 500 °C.

4.2.2. Gas Measurements

The gas sensor measurements of CuO nanowires were taken at lower temperatures in order to compare the sensor responses of pure CuO nanowires and P(S-*co*-CMS-C_{60}) @CuO hybrid structure. The P(S-*co*-CMS-C_{60}) can be deformed above the 100 C. CuO nanowires were tested against 1000 ppm H_2 gas at 30 °C, 50 °C, 100 °C and 5000 ppm Ethanol gas at 100 °C under dry air flow. The results of H_2 and ethanol measurements were showed at figure 4.14.

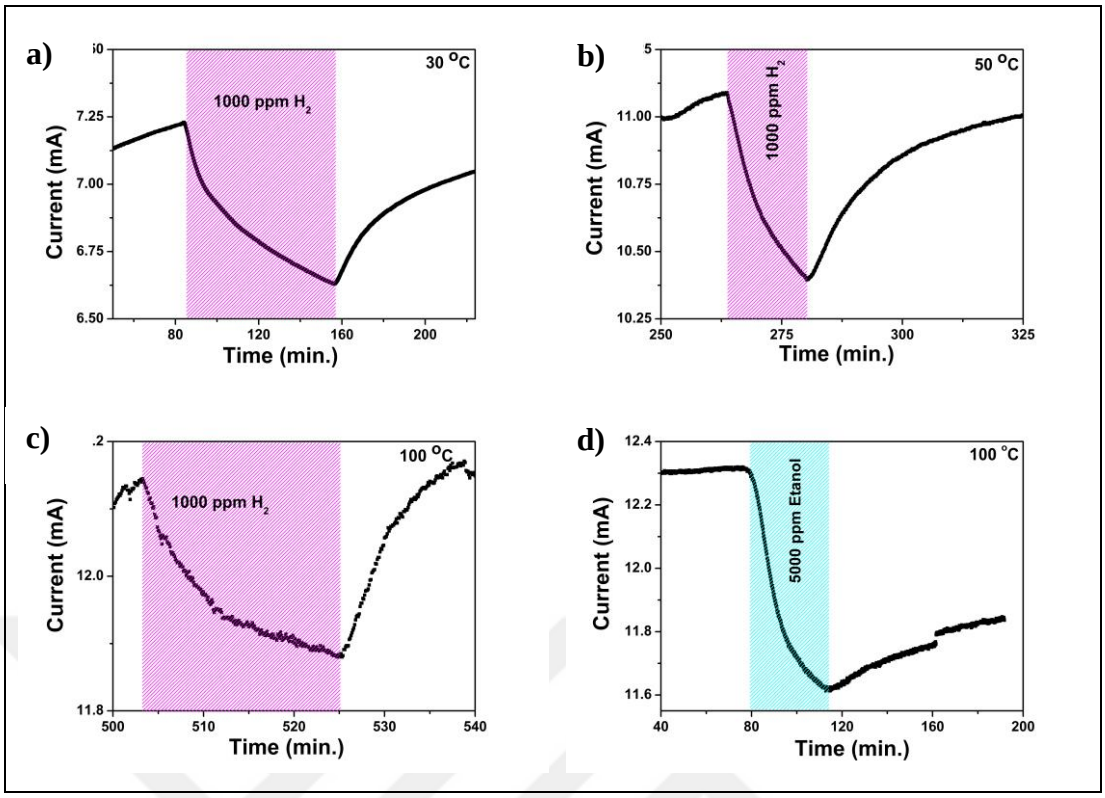

Figure 4.14: Sensor responses of CuO nanowires against 1000 ppm H_2 at a) 30 °C, b) 50 °C, c) 100 °C and d) against 5000 ppm ethanol at 100 °C.

According to these results, the recovery of CuO nanowires is a problem. Especially, there is no recovery for ethanol gas.

4.3. Organics@Cu_2O Nanowires Hybrid Structures

4.3.1. Structural Characterization

The SEM images were taken for the structural characterization of organics@Cu_2O nanowires hybrid structure to control the homogeneity of organic films on Cu_2O nanowires after spin coating. For the Cu_2O nanowires, homogeneity is not much because of the accumulation of Cu_2O nanowires locally during synthesis.

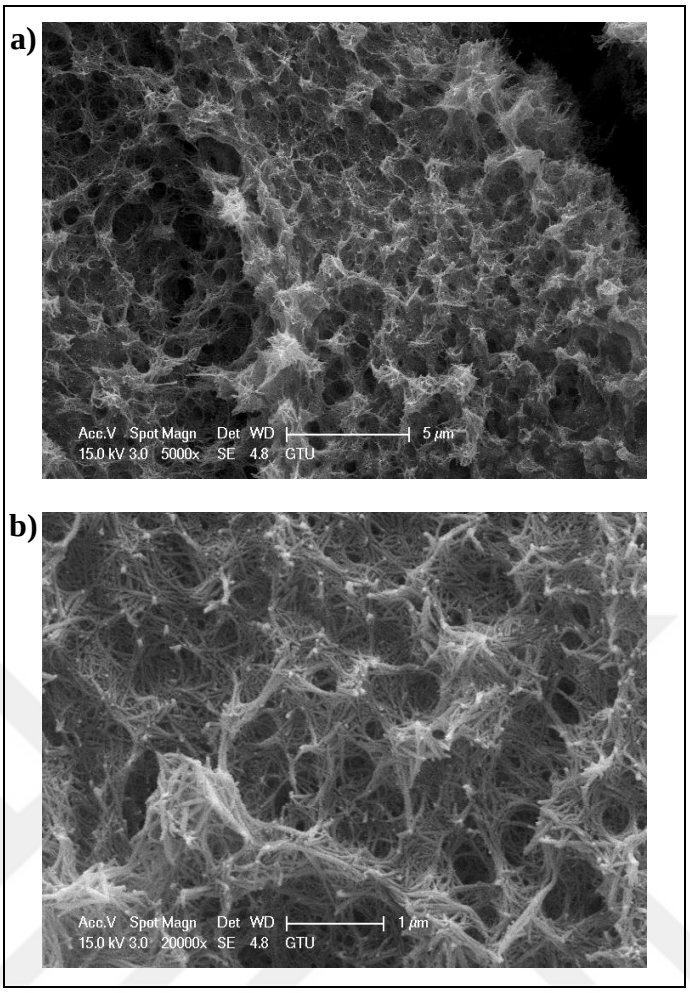

Figure 4.15: SEM images of the Zn-Pc@Cu_2O nanowires at different magnifications a) 5000X and b) 20000X.

4.3.2. Gas Measurements

The measurements of heterostructures of organics and Cu_2O nanowires were started with H_2 gas. The P(S-*co*-CMS-C_{60})@Cu_2O hybrid structures were tested against 1000 ppm H_2 gas under dry air flow at 30 °C, 50 °C, 100 °C and 150 °C. There was no response to H_2 gas at 30 °C and 50 °C. The sensor responses at 100 °C and 150 °C against 1000 ppm H_2 gas is given at figure 4.16.

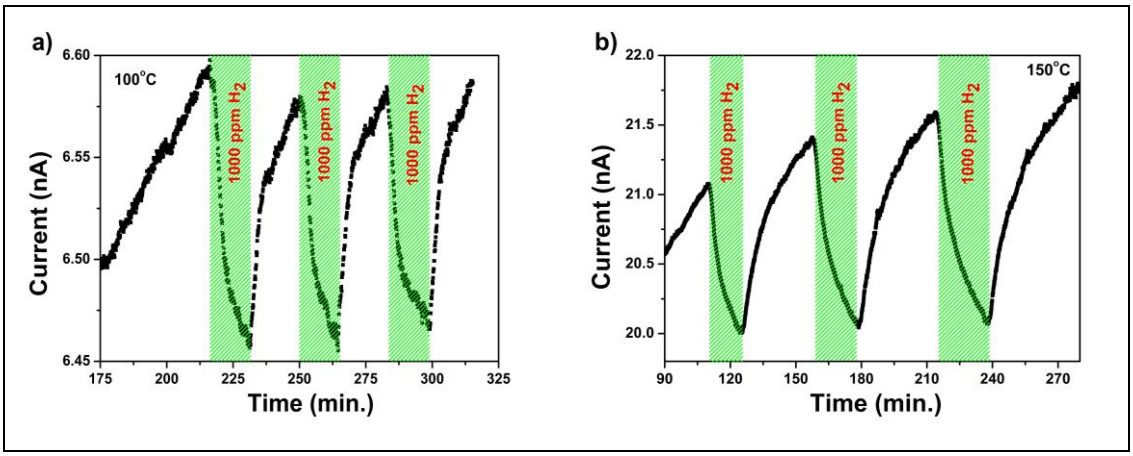

Figure 4.16: H_2 sensing of P(S-*co*-CMS-C_{60})@Cu_2O hybrid structures at a) 100 °C and b) 150 °C.

The results showed that base line of sensors have not observed for the P(S-*co*-CMS-C_{60})@Cu_2O hybrid structures. The reason may be that the hybrid structure can make the surface unstable.

The P(S-*co*-CMS-C_{60})@Cu_2O hybrid structure was tested against different concentrations of NO_2 gas at 23 °C, 50 °C and 100 °C. Some NO_2 sensor results were shown at figure 4.17. The results showed that increasing temperature enhance the NO_2 sensing of hybrid structure.

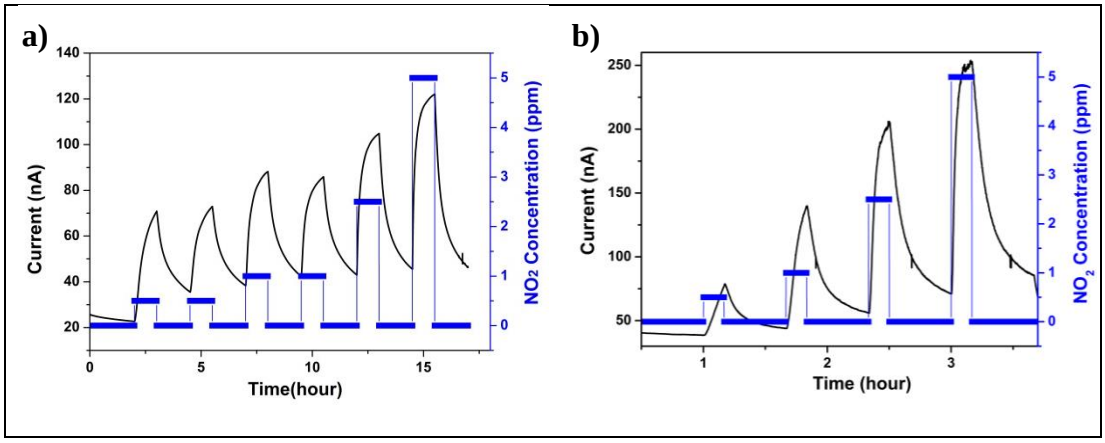

Figure 4.17: NO_2 measurements of P(S-*co*-CMS-C_{60})@Cu_2O hybrid structure at a) 23 °C and b) 150 °C.

Zn-Pc@Cu_2O hybrid structures were tested against 0.5 ppm, 1 ppm, 2.5 ppm, 5 ppm of NO_2 gas at 23 °C, 50 °C, 100 °C and 150 °C. Also, humidity effect on hybrid structure was investigated with measuring sensor response under %38 RH at 100 °C and 150 °C. Moreover, only Zn-Pc film sensor was tested against NO_2 gas at 100 °C

and 150 °C under dry air and %38 humid air flows to understand the effect of hybrid structures on NO_2 sensing. A comparison of sensor responses of only Zn-Pc film, only Cu_2O nanowires and their hybrid structures at 150 °C against different NO_2 concentrations is given at figure 4.18.

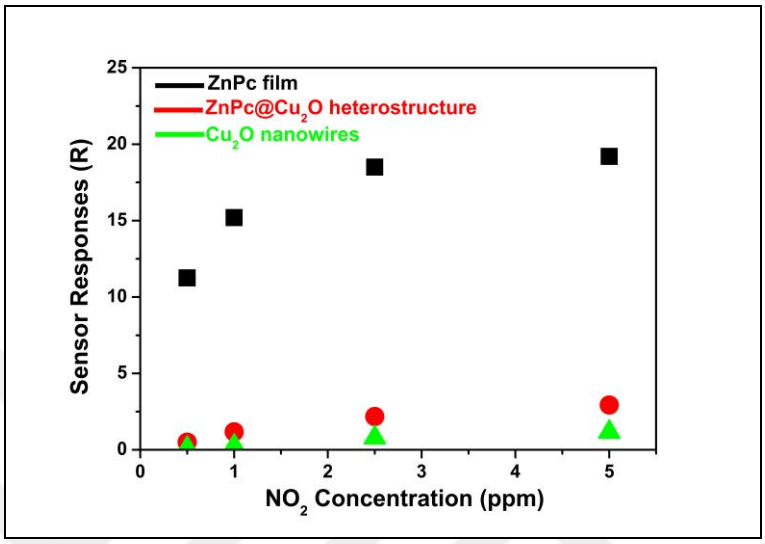

Figure 4.18: Response comparisons of ZnPc film and Cu_2O nanowires and their heterostructures against different NO_2 gas concentration at 150 °C under dry air flow.

According to figure 4.18., ZnPc film has the best response against NO_2 gas among other sensors. Moreover, ZnPc@Cu_2O hybrid structure showed better sensor response than Cu_2O nanostructures. The ZnPc film on Cu_2O nanowires enhanced the NO_2 sensing of Cu_2O nanowires. It is a significant result that there is not a big change on sensor responses beside the ZnPc film sensor response. This shows that Cu_2O nanowires are dominant on the sensing mechanism of heterostructure.

The humidity effect on NO_2 sensing of ZnPc film and ZnPc@Cu_2O hybrid structure was also investigated with measurements. Both samples were tested against 0.5 ppm, 1 ppm and 5 ppm NO_2 gas under %38 humid air flow. A comparison of sensor responses of ZnPc film and ZnPc@Cu_2O hybrid structure is given at figure 4.19.

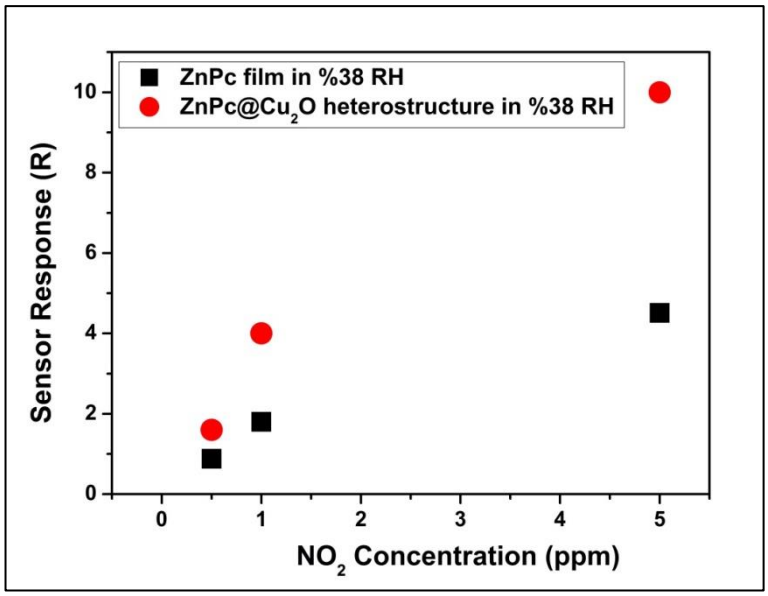

Figure 4.19: Response comparisons of ZnPc film and ZnPc@Cu_2O heterostructure under 38% RH.

The comparison at figure 4.19. shows that the hybrid structure has better NO_2 sensing than ZnPc film under humid air flow. The sensor response of ZnPc film was drastically decreased under humid air flow. This is well known property of organics that humidity has a negative effect on sensing. On the other hand, there is a significant increase on NO_2 sensing of ZnPc@Cu_2O hybrid structure. There is also an increase on NO_2 sensing of Cu_2O nanowires. Therefore, better sensing of hybrid structure is probably related with the bottom layer Cu_2O nanowires behavior against humidity discussed before. This is an important result to make better gas sensor under RH with organics@Cu_2O hybrid structures.

4.4. Organics@CuO Nanowires Hybrid Structures

4.4.1. Structural Characterization

The surface of P(S-*co*-CMS-C_{60})@CuO nanowires hybrid structure was investigated with SEM images to see the dispersion of organics on CuO nanowires. Figure 4.20. shows the SEM images of P(S-*co*-CMS-C_{60})@CuO nanowires hybrid structures.

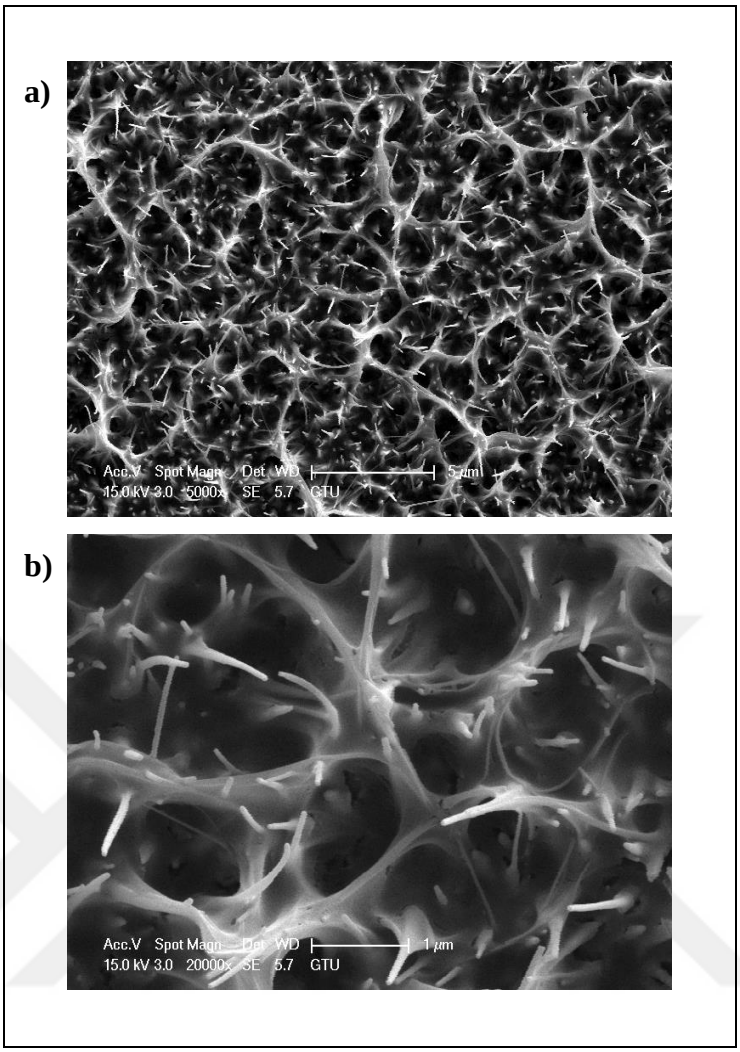

Figure 4.20: The SEM images of the P(S-*co*-CMS-C_{60})@CuO nanowires at different magnifications a) 5000X and b) 20000X.

Although the organics were diffused into the Cu_2O nanowires structure, P(S-*co*-CMS-C_{60}) spread as film structure over CuO nanowires. The homogeneity of CuO nanowires can be a reason for the protection of film structure of P(S-*co*-CMS-C_{60}).

4.4.2. Gas Measurements

The P(S-*co*-CMS-C_{60})@CuO hybrid structure was tested against 1000 ppm H_2 at 30 °C, 50 °C, 100 °C and 5000 ppm ethanol at 100 °C under dry air flow. Figure 4.21. shows the sensor responses of these measurements. There is not a big difference on H_2 sensing properties between 30 °C and 50 °C measurements for the CuO and P(S-*co*-CMS-C_{60})@CuO hybrid structures. On the other hand, there is an

enhancement on sensing properties of CuO with addition of P(S-*co*-CMS-C_{60}). The response and recovery times of P(S-*co*-CMS-C_{60})@CuO hybrid structure are faster than CuO nanowires against 1000 ppm H_2 gas at 100 °C.

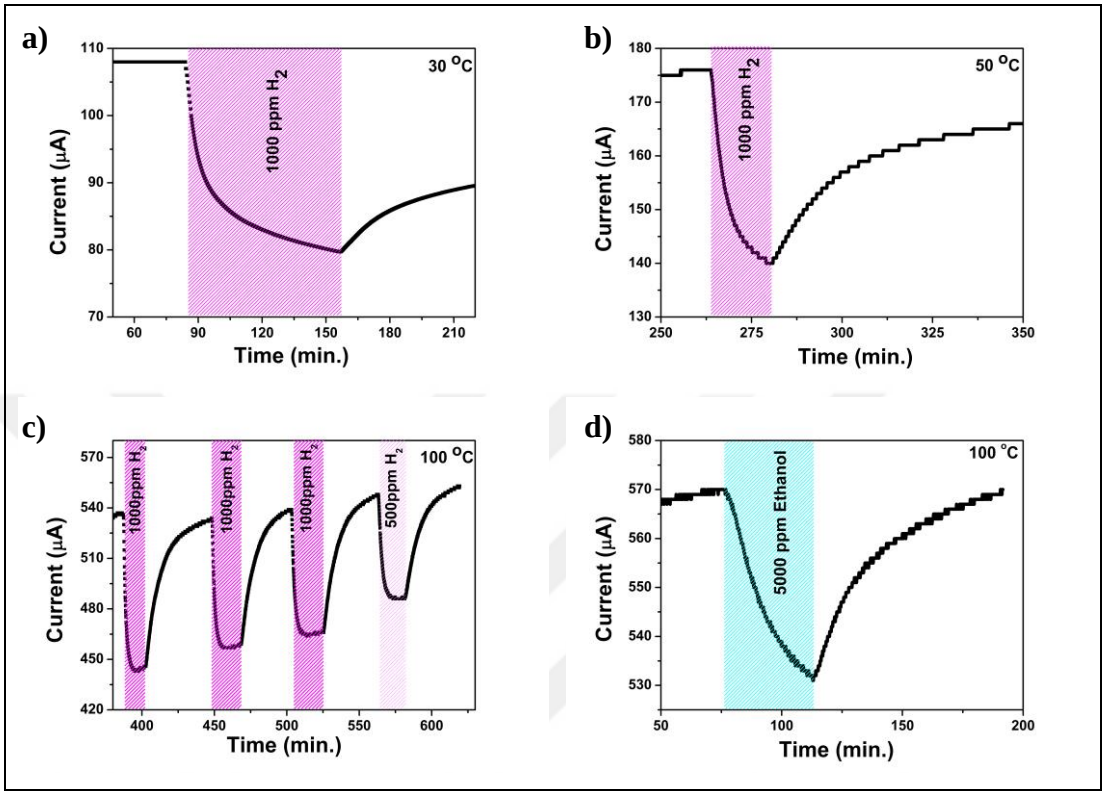

Figure 4.21: Sensor responses of P(S-*co*-CMS-C_{60})@CuO nanowires against 1000 ppm H_2 at a) 30 °C, b) 50 °C, c) 100 °C and d) against 5000 ppm ethanol at 100 °C.

5. CONCLUSIONS

In this work, Cu_2O nanowires and CuO nanowires were synthesized, characterized and tested against H_2, NO_2 in order to investigate the effect of organics@p-type semiconductor MOX hybrid structures on gas sensing properties. The main results were listed as;

- The Cu_2O nanowires were synthesized on glass substrate by vacuum annealing after Cu thin film anodization in KOH + NH_4F aqeous solution under 10 V potential for 5 minutes. The structural, optical and electrical characterizations of Cu2O were done by SEM, XRD and XPS measurements for structural, UV-vis absorption spectrum measurements for optical and DC electrical measurements at different temperatures for electrical characterization.
- The CuO nanowires were fabricated with thermal oxidation method on Si substrate. The structural characterizations were done by SEM and XRD measurements.
- The better working temperature of Cu_2O was determined as 200 °C with H2 sensing measurements.
- In NO_2 measurements, the response and recovery times are long for Cu_2O, organics and their heterostructures. Also, the full recovery of NO_2 is not observed for all samples at low temperatures.
- While the P(S-co-CMS-C_{60})@Cu_2O heterostructure showed better responses to NO_2 gas than pure Cu_2O nanowires at 150 °C, the P(S-co-CMS-C_{60}) film showed no responses to NO_2 gas at tested temperatures and concentrations.
- It was observed that Cu_2O nanowires, ZnPc film and their heterostructure have both ability to sense NO_2 in between 500ppb-5ppm concentration range at 23, 50, 100 and 150 °C temperatures. Also, while the response of ZnPc film is increasing with high temperatures, the response of Cu_2O nanowires and ZnPc@Cu_2O heterostructure is not increasing much.
- Besides the 38% relative humidity decreased drastically the sensor response of ZnPc film at 150 °C, it increased the sensor response of ZnPc@Cu_2O heterostructures against NO_2 gas. Also, ZnPc@Cu_2O heterostructure shows better sensing properties than ZnPc film in 38% RH.

- The H_2 sensing properties of CuO nanowires and P(S-co-CMS-C_{60})@CuO hybrid structures were compared with measurements. The hybrid structure decreased very much the response time of sensor.

REFERENCES

[1] Göpel W., Jones T. A., Kleitz M., Lundström I., Seiyama T., Hesse J., Zemel J. N., (2008), "Sensors, Chemical and Biochemical Sensors", 1st Edition, Wiley.

[2] Stetter J. R., Penrose W. R., (2002), "Understanding Chemical Sensors and Chemical Sensor Arrays (Electronic Noses): Past, Present, and Future", Sensors Update, 10 (1), 189-229.

[3] Heiland G., (1954), "Zum Einfluß von adsorbiertem Sauerstoff auf die elektrische Leitfähigkeit von Zinkoxydkristallen", Zeitschrift für Physik, 138 (3), 459-464.

[4] Bielanski A., Deren J., Haber J., (1957), "Electric conductivity and catalytic activity of semiconducting oxide catalysts", Nature, 179, 668-669.

[5] Seiyama T., Kagawa S., (1966), "Study on a Detector for Gaseous Components Using Semiconductive Thin Films", Analytical Chemistry, 38 (8), 1069-1073.

[6] Barsan N., Koziej D., Weimar U., (2007), "Metal oxide-based gas sensor research: How to? ", Sensors and Actuators B: Chemical, 121 (1), 18-35.

[7] Comini E., Baratto C., Faglia G., Ferroni M., Vomiero A., Sberveglieri G., (2009), "Quasi-one dimensional metal oxide semiconductors: Preparation, characterization and application as chemical sensors", Progress in Materials Science, 54 (1), 1-67.

[8] Arshak K., Gaidan I., (2005), "Development of a novel gas sensor based on oxide thick films", Materials Science and Engineering: B, 118 (1–3), 44-49.

[9] Ramgir N., Datta N., Kaur M., Kailasaganapathi S., Debnath A. K., Aswal D. K., Gupta S. K., (2013), "Metal oxide nanowires for chemiresistive gas sensors: Issues, challenges and prospects", Colloids and Surfaces A: Physicochemical and Engineering Aspects, 439, 101-116.

[10] Evans S. D., Johnson S. R., Cheng Y. L., Shen T., (2000), "Vapour sensing using hybrid organic-inorganic nanostructured materials", Journal of Materials Chemistry, 10 (1), 183-188.

[11] Kimura M., Sakai R., Sato S., Fukawa T., Ikehara T., Maeda R., Mihara T., (2012), "Sensing of Vaporous Organic Compounds by TiO2 Porous Films Covered with Polythiophene Layers", Advanced Functional Materials, 22 (3), 469-476.

[12] Guo X.-z., Kang Y.-f., Yang T.-l., Wang S.-r., (2012), "Low-temperature NO2 sensors based on polythiophene/WO3 organic-inorganic hybrids", Transactions of Nonferrous Metals Society of China, 22 (2), 380-385.

[13] Yamazoe N., (1991), "New approaches for improving semiconductor gas sensors", Sensors and Actuators B: Chemical, 5 (1), 7-19.

[14] Barsan N., Weimar U., (2001), "Conduction Model of Metal Oxide Gas Sensors", Journal of Electroceramics, 7 (3), 143-167.

[15] Comini E., (2006), "Metal oxide nano-crystals for gas sensing", Analytica Chimica Acta, 568 (1–2), 28-40.

[16] Yaacob M. H., Breedon M., Kalantar-zadeh K., Wlodarski W., (2009), "Absorption spectral response of nanotextured WO3 thin films with Pt catalyst towards H2", Sensors and Actuators B: Chemical, 137 (1), 115-120.

[17] Xia Y., Yang P., Sun Y., Wu Y., Mayers B., Gates B., Yin Y., Kim F., Yan H., (2003), "One-Dimensional Nanostructures: Synthesis, Characterization, and Applications", Advanced Materials, 15 (5), 353-389.

[18] Whitesides G., Mathias J., Seto C., (1991), "Molecular self-assembly and nanochemistry: a chemical strategy for the synthesis of nanostructures", Science, 254 (5036), 1312-1319.

[19] Comini E., Faglia G., Sberveglieri G., (2008), "Solid state gas sensing", 1st Edition, Springer Science & Business Media.

[20] Kim H.-J., Lee J.-H., (2014), "Highly sensitive and selective gas sensors using p-type oxide semiconductors: Overview", Sensors and Actuators B: Chemical, 192, 607-627.

[21] Choopun S. H., Wongrat, E., (2012), "Metal-Oxide Nanowires for Gas Sensors", 2012 Edition., Intech.

[22] Jiang T., Wang Y., Meng D., Wu X., Wang J., Chen J., (2014), "Controllable fabrication of CuO nanostructure by hydrothermal method and its properties", Applied Surface Science, 311, 602-608.

[23] Liu L., Hong K., Hu T., Xu M., (2012), "Synthesis of aligned copper oxide nanorod arrays by a seed mediated hydrothermal method", Journal of Alloys and Compounds, 511 (1), 195-197.

[24] Toboonsung B., Singjai P., (2011), "Formation of CuO nanorods and their bundles by an electrochemical dissolution and deposition process", Journal of Alloys and Compounds, 509 (10), 4132-4137.

[25] Wang X., Li C., Chen G., He L., Cao H., Zhang B., (2011), "Selective fabrication of Cu/Cu2O nanowires using porous alumina membranes in acidic solution", Solid State Sciences, 13 (1), 280-284.

[26] Chen M.-J., Wu C.-Y., Kuo Y.-M., Chen H.-Y., Tsai C.-H., (2012), "Preparation of Cu2O nanowires by thermal oxidation-plasma reduction method", Applied Physics A, 108 (1), 133-141.

[27] Zhang Z., Zhong C., Liu L., Teng X., Wu Y., Hu W., (2015), "Electrochemically prepared cuprous oxide film for photo-catalytic oxygen evolution from water oxidation under visible light", Solar Energy Materials and Solar Cells, 132, 275-281.

[28] Zhang Z., Zhong C., Deng Y., Liu L., Wu Y., Hu W., (2013), "The manufacture of porous cuprous oxide film with photocatalytic properties via an electrochemical-chemical combination method", RSC Advances, 3 (19), 6763-6766.

[29] Xufeng Wu H. B., Jiaxin Zhang, Feng'en Chen, and Gaoquan Shi, (2005), "Copper Hydroxide Nanoneedle and Nanotube Arrays Fabricated by Anodization of Copper", Journal of Physical Chemistry, 109 (49), 22836-22842.

[30] Allam N. K., Grimes C. A., (2011), "Electrochemical fabrication of complex copper oxide nanoarchitectures via copper anodization in aqueous and non-aqueous electrolytes", Materials Letters, 65 (12), 1949-1955.

[31] Zhang Q., Zhang K., Xu D., Yang G., Huang H., Nie F., Liu C., Yang S., (2014), "CuO nanostructures: Synthesis, characterization, growth mechanisms, fundamental properties, and applications", Progress in Materials Science, 60, 208-337.

[32] Kim Y.-S., Hwang I.-S., Kim S.-J., Lee C.-Y., Lee J.-H., (2008), "CuO nanowire gas sensors for air quality control in automotive cabin", Sensors and Actuators B: Chemical, 135 (1), 298-303.

[33] Raksa P., Gardchareon A., Chairuangsri T., Mangkorntong P., Mangkorntong N., Choopun S., (2009), "Ethanol sensing properties of CuO nanowires prepared by an oxidation reaction", Ceramics International, 35 (2), 649-652.

[34] Wang Y., Shen R., Jin X., Zhu P., Ye Y., Hu Y., (2011), "Formation of CuO nanowires by thermal annealing copper film deposited on Ti/Si substrate", Applied Surface Science, 258 (1), 201-206.

[35] Barreca D., Fornasiero P., Gasparotto A., Gombac V., Maccato C., Montini T., Tondello E., (2009), "The potential of supported Cu2O and CuO nanosystems in photocatalytic H2 production", ChemSusChem, 2 (3), 230-233.

[36] Zhang J., Liu J., Peng Q., Wang X., Li Y., (2006), "Nearly Monodisperse Cu2O and CuO Nanospheres: Preparation and Applications for Sensitive Gas Sensors", Chemistry of Materials, 18 (4), 867-871.

[37] Zhang H., Zhu Q., Zhang Y., Wang Y., Zhao L., Yu B., (2007), "One-Pot Synthesis and Hierarchical Assembly of Hollow Cu2O Microspheres with Nanocrystals-Composed Porous Multishell and Their Gas-Sensing Properties", Advanced Functional Materials, 17 (15), 2766-2771.

[38] Gasparotto A., Barreca D., Fornasiero P., Gombac V., Lebedev O., Maccato C., Montini T., Tondello E., Van Tendeloo G., Comini E., Sberveglieri G., (2009), "Multi-Functional Copper Oxide Nanosystems for H2 Sustainable Production and Sensing", ECS Transactions, 25 (8), 1169-1176.

[39] Guan L., Pang H., Wang J., Lu Q., Yin J., Gao F., (2010), "Fabrication of novel comb-like Cu2O nanorod-based structures through an interface etching method and their application as ethanol sensors", Chemical Communications, 46 (37), 7022-7024.

[40] Zoolfakar A. S., Ahmad M. Z., Rani R. A., Ou J. Z., Balendhran S., Zhuiykov S., Latham K., Wlodarski W., Kalantar-zadeh K., (2013), "Nanostructured copper oxides as ethanol vapour sensors", Sensors and Actuators B: Chemical, 185, 620-627.

[41] Muzikante I., Parra V., Dobulans R., Fonavs E., Latvels J., Bouvet M., (2007), "A Novel Gas Sensor Transducer Based on Phthalocyanine Heterojunction Devices", Sensors, 7 (11), 2984.

[42] Forrest S. R., (1997), "Ultrathin Organic Films Grown by Organic Molecular Beam Deposition and Related Techniques", Chemical Reviews, 97 (6), 1793-1896.

[43] Wright J. D., (1989), "Gas adsorption on phthalocyanines and its effects on electrical properties", Progress in Surface Science, 31 (1), 1-60.

[44] Bouvet M., (2006), "Phthalocyanine-based field-effect transistors as gas sensors", Anal Bioanal Chem, 384 (2), 366-373.

[45] Chen X., Wong C. K. Y., Yuan C. A., Zhang G., (2013), "Nanowire-based gas sensors", Sensors and Actuators B: Chemical, 177, 178-195.

[46] Chen X., Yuan C. A., Wong C. K. Y., Ye H., Leung S. Y. Y., Zhang G., (2012), "Molecular modeling of protonic acid doping of emeraldine base polyaniline for chemical sensors", Sensors and Actuators B: Chemical, 174, 210-216.

[47] Chen X., Wong C. K. Y., Yuan C. A., Zhang G., (2012), "Impact of the functional group on the working range of polyaniline as carbon dioxide sensors", Sensors and Actuators B: Chemical, 175, 15-21.

[48] Diaz A. F., Rubinson J. F., Mark H. B., (1988), "Electrochemistry and electrode applications of electroactive/conductive polymers", Advances in Polymer Science, 84, 113-139.

[49] Bai H., Shi G., (2007), “Gas Sensors Based on Conducting Polymers”, Sensors (Basel, Switzerland), 7 (3), 267-307.

[50] Chen X. P., Yuan C. A., Wong C. K. Y., Koh S. W., Zhang G. Q., (2011), “Validation of forcefields in predicting the physical and thermophysical properties of emeraldine base polyaniline”, Molecular Simulation, 37 (12), 990-996.

[51] Bartlett P. N., Ling-Chung S. K., (1989), “Conducting polymer gas sensors Part III: Results for four different polymers and five different vapours”, Sensors and Actuators, 20 (3), 287-292.

[52] Marsella M. J., Carroll P. J., Swager T. M., (1995), “Design of chemoresistive sensory materials: polythiophene-based pseudopolyrotaxanes”, Journal of the American Chemical Society, 117 (39), 9832-9841.

[53] Bruschi P., Cacialli F., Nannini A., Neri B., (1994), “Gas and vapour effects on the resistance fluctuation spectra of conducting polymer thin-film resistors”, Sensors and Actuators B: Chemical, 19 (1), 421-425.

[54] Torsi L., Pezzuto M., Siciliano P., Rella R., Sabbatini L., Valli L., Zambonin P. G., (1998), “Conducting polymers doped with metallic inclusions: New materials for gas sensors”, Sensors and Actuators B: Chemical, 48 (1–3), 362-367.

[55] Hirata M., Sun L., (1994), “Characteristics of an organic semiconductor polyaniline film as a sensor for NH3 gas”, Sensors and Actuators A: Physical, 40 (2), 159-163.

[56] Unde S., Ganu J., Radhakrishnan S., (1996), “Conducting polymer-based chemical sensor: Characteristics and evaluation of polyaniline composite films”, Advanced Materials for Optics and Electronics, 6 (3), 151-157.

[57] Ogura K., Saino T., Nakayama M., Shiigi H., (1997), “The humidity dependence of the electrical conductivity of a solublepolyaniline-poly(vinyl alcohol) composite film”, Journal of Materials Chemistry, 7 (12), 2363-2366.

[58] Park Y. H., Han M. H., (1992), “Preparation of conducting polyacrylonitrile/polypyrrole composite films by electrochemical synthesis and their electrical properties”, Journal of Applied Polymer Science, 45 (11), 1973-1982.

[59] Wang H. L., Toppare L., Fernandez J. E., (1990), “Conducting polymer blends: polythiophene and polypyrrole blends with polystyrene and poly(bisphenol A carbonate) ”, Macromolecules, 23 (4), 1053-1059.

[60] Adhikari B., Majumdar S., (2004), “Polymers in sensor applications”, Progress in Polymer Science, 29 (7), 699-766.

[61] Tang C. W., (1986), “Two-layer organic photovoltaic cell”, Applied Physics Letters, 48 (2), 183-185.

[62] Sicot L., Geffroy B., Lorin A., Raimond P., Sentein C., Nunzi J.-M., (2001), “Photovoltaic properties of Schottky and p–n type solar cells based on polythiophene”, Journal of Applied Physics, 90 (2), 1047-1054.

[63] Gökçeören A. T., Kaplan E., Arslanoğlu Y., (2014), “Electrochemical and morphological analysis on novel phthalocyanine grafted conductive polymeric nanofibers”, Journal of Electroanalytical Chemistry, 729, 87-94.

[64] Cole A., McIlroy R. J., Thorpe S. C., Cook M. J., McMurdo J., Ray A. K., (1993), “Substituted phthalocyanine gas sensors”, Sensors and Actuators B: Chemical, 13 (1), 416-419.

[65] Lai S. L., Chan M. Y., Fung M. K., Lee C. S., Lee S. T., (2007), “Copper hexadecafluorophthalocyanine and copper phthalocyanine as a pure organic connecting unit in blue tandem organic light-emitting devices”, Journal of Applied Physics, 101 (1), 014509.

[66] Bouvet M., Leroy A., Simon J., Tournilhac F., Guillaud G., Lessnick P., Maillard A., Spirkovitch S., Debliquy M., de Haan A., Decroly A., (2001), “Detection and titration of ozone using metallophthalocyanine based field effect transistors”, Sensors and Actuators B: Chemical, 72 (1), 86-93.

[67] Krier A., Azim-Araghi M. E., (1997), “The influence of NO2 on the conductivity of chloro-aluminium phthalocyanine thin films”, Journal of Physics and Chemistry of Solids, 58 (5), 711-716.

[68] Kılınç N., Atilla D., Öztürk S., Gürek A. G., Öztürk Z. Z., Ahsen V., (2009), “Oxidizing gas sensing properties of mesogenic copper octakisalkylthiophthalocyanine chemoresistive sensors”, Thin Solid Films, 517 (22), 6206-6210.

[69] Kılınç N., Öztürk S., Atilla D., Gürek A. G., Ahsen V., Öztürk Z. Z., (2012), “Electrical and NO2 sensing properties of liquid crystalline phthalocyanine thin films”, Sensors and Actuators B: Chemical, 173, 203-210.

[70] Öztürk Z. Z., Zhou R., Weimar U., Ahsen V., Bekaroglu Ö., Göpel W., (1995), “Soluble phthalocyanines for the detection of organic solvents: thin film structures with quartz microbalance and capacitance transducers”, Sensors and Actuators B: Chemical, 26 (1), 208-212.

[71] Kılınç N., Atilla D., Gürek A. G., Öztürk Z. Z., Ahsen V., (2009), “Volatile organic compounds sensing properties of tetrakis(alkylthio)-substituted lutetium(III) bisphthalocyanines thin films”, Talanta, 80 (1), 263-268.

[72] Altindal A., Öztürk Z. Z., Dabak S., Bekaroğlu Ö., (2001), “Halogen sensing using thin films of crosswise-substituted phthalocyanines”, Sensors and Actuators B: Chemical, 77 (1–2), 389-394.

[73] Urban G., Wöllenstein J., Kieninger J., Şişman O., Kılınç N., Öztürk Z. Z., (2015), "Eurosensors 2015H2 Sensing Properties of Cu2O Nanowires on Glass Substrate", Procedia Engineering, 120, 1170-1174.

[74] Zhong J.-H., Li G.-R., Wang Z.-L., Ou Y.-N., Tong Y.-X., (2011), "Facile Electrochemical Synthesis of Hexagonal Cu2O Nanotube Arrays and Their Application", Inorganic Chemistry, 50 (3), 757-763.

[75] Poulston S., Parlett P. M., Stone P., Bowker M., (1996), "Surface Oxidation and Reduction of CuO and Cu2O Studied Using XPS and XAES", Surface and Interface Analysis, 24 (12), 811-820.

[76] Ma L., Lin Y., Wang Y., Li J., Wang E., Qiu M., Yu Y., (2008), "Aligned 2-D Nanosheet Cu2O Film: Oriented Deposition on Cu Foil and Its Photoelectrochemical Property", The Journal of Physical Chemistry C, 112 (48), 18916-18922.

[77] Yang Y., Han J., Ning X., Cao W., Xu W., Guo L., (2014), "Controllable Morphology and Conductivity of Electrodeposited Cu2O Thin Film: Effect of Surfactants", ACS Applied Materials & Interfaces, 6 (24), 22534-22543.

[78] Zheng Z., Huang B., Wang Z., Guo M., Qin X., Zhang X., Wang P., Dai Y., (2009), "Crystal Faces of Cu2O and Their Stabilities in Photocatalytic Reactions", The Journal of Physical Chemistry C, 113 (32), 14448-14453.

[79] Pan L., Zou J.-J., Zhang T., Wang S., Li Z., Wang L., Zhang X., (2014), "Cu2O Film via Hydrothermal Redox Approach: Morphology and Photocatalytic Performance", The Journal of Physical Chemistry C, 118 (30), 16335-16343.

[80] Lefèvre G., Walcarius A., Ehrhardt J. J., Bessière J., (2000), "Sorption of Iodide on Cuprite (Cu2O) ", Langmuir, 16 (10), 4519-4527.

[81] Dong C., Zhong H., Kou T., Frenzel J., Eggeler G., Zhang Z., (2015), "Three-Dimensional Cu Foam-Supported Single Crystalline Mesoporous Cu2O Nanothorn Arrays for Ultra-Highly Sensitive and Efficient Nonenzymatic Detection of Glucose", ACS Appl Mater Interfaces, 7 (36), 20215-20223.

[82] Sung S.-Y., Kim S.-Y., Jo K.-M., Lee J.-H., Kim J.-J., Kim S.-G., Chai K.-H., Pearton S. J., Norton D. P., Heo Y.-W., (2010), "Fabrication of p-channel thin-film transistors using CuO active layers deposited at low temperature", Applied Physics Letters, 97 (22), 222109.

[83] Singh D. P., Neti N. R., Sinha A. S. K., Srivastava O. N., (2007), "Growth of Different Nanostructures of Cu2O (Nanothreads, Nanowires, and Nanocubes) by Simple Electrolysis Based Oxidation of Copper", The Journal of Physical Chemistry C, 111 (4), 1638-1645.

[84] Singh B., Mehta B. R., (2014), "Relationship between nature of metal-oxide contacts and resistive switching properties of copper oxide thin film based devices", Thin Solid Films, 569, 35-43.

[85] Tan Y., Xue X., Peng Q., Zhao H., Wang T., Li Y., (2007), "Controllable Fabrication and Electrical Performance of Single Crystalline Cu2O Nanowires with High Aspect Ratios", Nano Letters, 7 (12), 3723-3728.

[86] Kaur M., Muthe K. P., Despande S. K., Choudhury S., Singh J. B., Verma N., Gupta S. K., Yakhmi J. V., (2006), "Growth and branching of CuO nanowires by thermal oxidation of copper", Journal of Crystal Growth, 289 (2), 670-675.

[87] Shao P., Deng S., Chen J., Xu N., (2011), "Large-scale fabrication of ordered arrays of microcontainers and the restraint effect on growth of CuO nanowires", Nanoscale Research Letters, 6 (1), 86-86.

[88] Gonçalves A. M. B., Campos L. C., Ferlauto A. S., Lacerda R. G., (2009), "On the growth and electrical characterization of CuO nanowires by thermal oxidation", Journal of Applied Physics, 106 (3), 034303.

[89] Zhong M. L., Zeng D. C., Liu Z. W., Yu H. Y., Zhong X. C., Qiu W. Q., (2010), "Synthesis, growth mechanism and gas-sensing properties of large-scale CuO nanowires", Acta Materialia, 58 (18), 5926-5932.

[90] Yuan L., Wang Y., Mema R., Zhou G., (2011), "Driving force and growth mechanism for spontaneous oxide nanowire formation during the thermal oxidation of metals", Acta Materialia, 59 (6), 2491-2500.

BIOGRAPHY

Orhan Şişman was born in 1989 in Kocaeli, Turkey. He obtained the degree of Master of Science without thesis from 5 years integrated program in Physics Education at Middle East Technical University (METU) in 2013. In METU, he accomplished Test and Measurement package in Physics Department with restricted selective courses.

In September 2013, he joined the group of Prof. Z.Ziya Ozturk at the Graduate School of Natural and Applied Sciences, Physics Department of the Gebze Technical University. He started to study on synthesis of AAO nanopores template for ZnO nanorods fabrication in the project "Development of Automotive Gas Sensors Based on Nano-Metal-Oxide Semiconductor with increased Selectivity, Sensitivity and Stability" (project number "111M261") supported by the Scientific and Technological Research Council of Turkey (TUBITAK). Then, his research interests shifted to fabrication, characterization, electrical and gas sensing properties of nanostructured CuO, Cu_2O and their hybrid structures with organics by the Cost Action Project "Fabrication, characterization and investigation of gas sensing properties of metal oxide/organic nano-heterostructures". He was research assistant in this project. The project director is Assoc. Prof. Necmettin Kilinc who is MC substitute in MPNS COST Action MP 1202. In a part of this project, he found chance to work in STSM (Short Term Scientific Mission) program with Prof. Albert Romano Rodriguez in Barcelona University on NO_2 sensing properties of organic@Cu_2O nanowires heterostructure.

APPENDICES

Appendix A: Publications During This Thesis

Sisman O., Kilinc N., Ozturk Z.Z., (2015), "H_2 Sensing Properties of Cu_2O Nanowires on Glass Substrate", Procedia Engineering 120, 1170-1174.